

AD-R167 540

A THIN FILM COATING PLANT USING THICKNESS MONITORING
(U) AIR FORCE INST OF TECH WRIGHT-PATTERSON AFB OH
SCHOOL OF ENGINEERING J J ERIC DEC 84

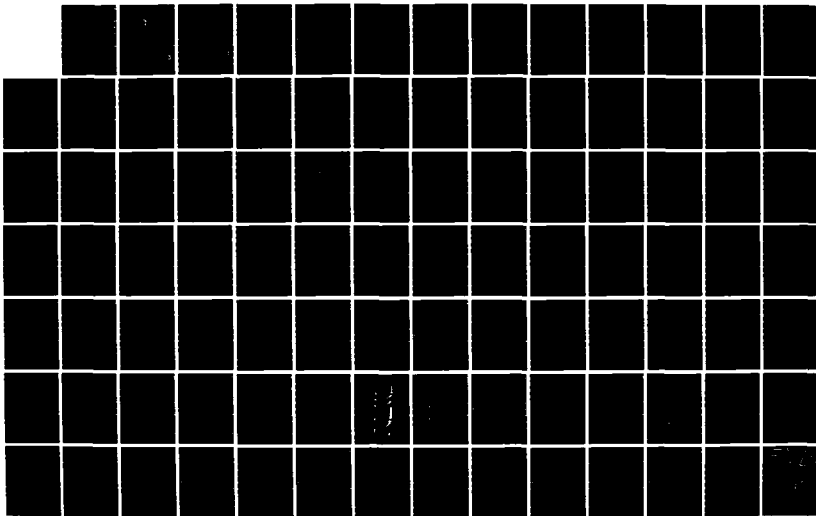
1/1

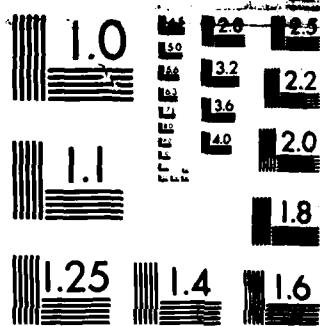
UNCLASSIFIED

AFIT/GEP/PH/84-D-3

F/G 11/3

NL



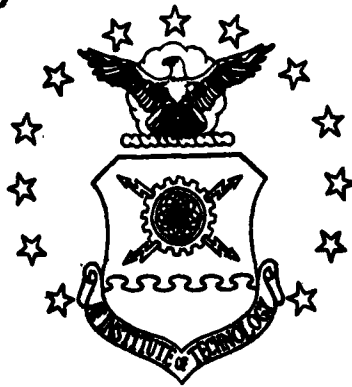


MICROCOPY RESOLUTION TEST CHART
NATIONAL BUREAU OF STANDARDS-1963-A

1

AD-A167 540

AIR FORCE INSTITUTE OF TECHNOLOGY



AIR UNIVERSITY
UNITED STATES AIR FORCE

A THIN FILM COATING PLANT
USING THICKNESS MONITORING

THESIS

AFIT/GEP/PH/84-D-3 John J. Er
1st Lt US

DTIC FILE COPY

SCHOOL OF ENGINEERING

DTIC
ELECTE
MAY 12 1986

S D
B

WRIGHT-PATTERSON AIR FORCE BASE, OHIO

DISTRIBUTION STATEMENT A
Approved for public release
Distribution Unlimited

86 5 12 038

AFIT/GEP/PH/84-D-3

①

AD-A167540

A THIN FILM COATING PLANT
USING THICKNESS MONITORING

THESIS

AFIT/GEP/PH/84-D-3

John J. Eric
1st Lt USAF

S DTIC ELECTE **D**
MAY 12 1986
B

Approved for public release; distribution unlimited

AFIT/GEP/PH/84-D-3

A THIN FILM COATING PLANT USING
THICKNESS MONITORING

THESIS

Presented to the Faculty of the School of Engineering
of the Air Force Institute of Technology

Air University

In Partial Fulfillment of the
Requirements for the Degree of
Master of Science

John J. Eric, B.S.
First Lieutenant, USAF

December 1984

Approved for public release; distribution unlimited

Acknowledgements

During the course of this thesis project, I have received help from many sources to which I am grateful. I would like to thank my thesis committee, consisting of Maj John Wharton, my advisor; Dr. Robert Hengehold; and Lt Col Howard Evans for their advice and assistance. Special thanks goes to Mr. Curtis Atnipp for all the help locating needed equipment and then making it work properly. Sincere appreciation goes to the members of the School Shop for parts fabrications done so well and so quickly, and to members of the Avionics Lab Integrated Circuit Facility for the loan of a desperately needed quartz sensor. Most of all, I wish to thank Kimberly, my wife, for putting up with me through all of this and for the support and understanding that helped so much.

John J. Eric



Accession #	
NTIS GRA&I	<input checked="" type="checkbox"/>
DTIC TAB	<input type="checkbox"/>
Unannounced	<input type="checkbox"/>
Justification	
By	
Date	
A-1	

Contents

	Page
Acknowledgements.....	ii
List of Figures.....	iv
List of Tables.....	vi
Notation.....	vii
Abstract.....	viii
I. Introduction.....	1
II. Vapor Deposition.....	3
Vacuum Evaporation.....	3
Vacuum Deposition of Films.....	4
Source Emission and Film Thickness Distribution	7
III. Vacuum Deposition System.....	16
General.....	16
Bell Jar System.....	16
Gas Flow.....	16
Roughing Pump.....	18
High Vacuum Pump.....	21
Vacuum Gauges.....	23
Electron Gun Source.....	24
IV. Optical Monitoring of Film Thickness.....	27
Theory - Quarter Wave Films.....	27
Absorption Effects.....	38
Changes in Films Due to Packing of the Deposit and Moisture Absorption.....	40
V. Quartz Crystal Monitoring.....	44
Theory and Operation.....	44
Sensitivity and Accuracy.....	51
Long Term Operation and Linearity.....	52
Optimum Usage of Quartz Crystal Oscillators...	56
VI. Experimental Arrangement.....	58
VII. Results.....	64
VIII. Conclusion and Recommendations.....	73
Appendix: Derivation of the Characteristic Matrix for a Thin Film.....	76
Bibliography.....	81
Vita.....	83

List of Figures

Figure	Page
1. Evaporation Source Geometry.....	8
2. Evaporation onto a Plane Substrate.....	10
3. Thickness Distribution on a Plane Surface.....	13
4. Arrangement for Knudsen's Proof of the Cosine Law	13
5. Substrate Holder.....	15
6. Bell Jar Vacuum System.....	17
7. VacSorb [®] Pump.....	19
8. VacIon [®] Pumping Element.....	22
9. Electron Beam Gun.....	25
10. The Admittance Locus.....	32
11. Admittance Diagram with constant δ contours Added	33
12. Admittance Locus with constant δ contours and Iso-reflectance contours Added.....	35
13. Variation of Reflectance with Film Thickness.....	36
14. Trend of Transmission Signal Toward Zero for Many-Layered Deposition.....	41
15. AT-cut Quartz Crystal.....	45
16. Frequency Change vs Temperature for AT-cut Crystal	45
17. Sloan Instruments Water-Cooled Quartz Crystal Sensor.....	49
18. Optical Monitoring System.....	58
19. Optical Path Through System.....	60
20. Optical Monitor Response Test with White Light Source.....	65
21. Optical Monitor Response Test with He-Ne Laser....	66
22. Optical Monitor Output for TiO ₂ Deposition Run....	70
23. Interaction of Radiation with Film-Substrate Combination.....	76

Figure

Page

24. \bar{H} and \bar{E} waves within the Film Thickness..... 78

List of Tables

Table	Page
I. Sensitivity for Some Specific Starting Frequencies	51
II. Permitted Frequency Shifts for Some Specified Starting Frequencies.....	54

Notation

A = active area of quartz crystal

C = conductance

d_j = physical thickness of j^{th} layer

D_j = optical thickness of j^{th} layer

δ = phase thickness

dS_2 = substrate surface area

\bar{E} = electric field

f = frequency

\bar{H} = magnetic field

L = mean free path

m_1 = mass emitted by source

m_2 = mass received by substrate

N_j = index of refraction of j^{th} layer

p = pressure

Q = gas flow rate, throughput

R = reflectance

ρ = density

S_p = pump speed

Ω = solid angle

t = thickness

T = transmittance

V = volume

λ = wavelength

Y = optical admittance

Abstract

The purpose of this thesis project was to modify an existing vacuum system into a thin film coating plant which would also employ film thickness monitoring that could be carried out during film deposition for proper control and termination of the process. The thickness monitoring processes employed were the optical method of turning value monitoring, and quartz crystal oscillator frequency monitoring. The results indicated that these two methods responded in the expected manner when a film of TiO_2 was deposited, however, the actual values for the oscillator frequency change and the transmittance at the turning point were not those expected. These errors could be due to a different crystal cut other than AT, or a change in the material index of refraction or chemical composition upon evaporation and subsequent condensation at the substrate. It was recommended, based on the work done during the project, that various equipment upgrades be made and further test deposition runs be accomplished in order to correlate the output of the two monitoring systems.

I Introduction

Instruments and equipment using optical components such as lenses and mirrors are finding increased application in areas such as laser technology, optical communications, and surveillance, to name a few. Specific performance demands on the characteristics of various optical systems will create further demands on their basic optical components. Lasers, for example, usually operating at a single wavelength or in a very narrow bandwidth, have a cavity that requires optical components that will keep enough of the radiation inside the cavity in support of the lasing process, yet allow transmission of a portion of the radiation in the form of the laser beam. For instruments such as surveillance equipment that may be used at night or in low-light-level conditions, the optical components that make up the system must be able to pass on to the receiver or observer as much of the available light collected from the source as is possible. This can be done, for example, by lowering the reflectance of the lenses so that the maximum amount of light will be transmitted.

The reflectance of a substance depends on the index of refraction, a property of the material. For glass, the reflectance is about 4% at each surface, but this can be changed by the application of a thin film optical coating onto the glass surface. Deposition of thin film coatings on glass and other materials can produce the performance characteristics required in advanced optical systems. Coatings can be made that are nearly totally reflecting, antireflecting,

or somewhere in between.

Advances in optical technology and the interest in investigating optical techniques in the laboratory provide good reason for the benefits of having the capability to produce optically coated elements for testing in the AFIT labs or for use in student research projects. Development of a thin film coating plant can provide this capability.

The object of this thesis project has been the modification and return to operation of the vacuum coating chamber in the AFIT Physics Department Lab and investigation of film thickness monitors to be used during the film deposition process. Film thickness monitors can measure either optical thickness (film thickness as seen by the incoming radiation) or physical thickness (actual geometrical thickness) and thus allow for control of the deposition of the film. Termination of film deposition can be made when the desired optical characteristics are obtained. These monitoring systems will then be employed in the operation of the coating plant.

Following this introduction, Chapter II describes the vapor deposition process while the vacuum system in which this occurs is discussed in Chapter III. Chapters IV and V present the theory and operation of the optical monitoring system and the quartz crystal monitoring system, respectively. The arrangement employing these systems in the coating plant are described in Chapter VI, test results are provided in Chapter VII, and conclusions and subsequent recommendations are given in Chapter VIII.

II Vapor Deposition

A. Vacuum Evaporation

Vacuum evaporation is the process by which a material is heated in a vacuum environment resulting in a large number of atoms or molecules escaping the surface of the substance to form a vapor. The heating may be accomplished by resistance heating of the material's container, heating the material in turn by conduction, or by electron bombardment, in which the material is heated directly by high-energy electrons. A vacuum environment of very low pressure is used so that the atoms or molecules in the atmosphere remaining in the chamber are so few so as to undergo no collisions with those of the vapor. These collisions would have the effect of interfering with the vapor's direction of flow or causing contamination of the vapor by mixing or chemically combining with it. The vapor produced in a vacuum evaporation process is then most often used to deposit a thin coating of the material on some other substance by condensing on its surface.

Among the advantages of coating materials using vacuum evaporation (8;2-3) are that either metals or non-metals may be coated, thickness can be controlled to closer limits than with other methods, and uniform coatings can be produced on items of various or complicated shapes.

Disadvantages of the vacuum evaporation method include obtaining the required pressures for the process, usually 5×10^{-4} torr or less; obtaining these pressures when using very volatile materials; and providing materials sufficiently

clean for the deposit to adhere to (8;2-3). The main topic of this investigation, thickness monitoring techniques, is also a significant problem.

B. Vacuum Deposition of Films

The vapor used to deposit a thin film on a substrate is produced when a substance is heated by the addition of a quantity of energy known as the heat of vaporization. Most of this energy is involved with overcoming the mutual attraction that the atoms or molecules in the substance have for each other. Once enough energy is added to escape the attraction of the substance, molecules (or atoms) are released from the material's surface with a kinetic energy that is only a fraction of the initial energy input. (4;117-118)

The number of gas molecules per unit volume is given from the ideal gas law by:

$$n = \frac{N}{V} = \frac{p}{kT} \quad (1)$$

If pressure were expressed in torr and n is in molecules per cubic centimeter, then (4;21)

$$n = 9.656 \times 10^{18} \frac{p}{T} \quad (2)$$

Starting with the vacuum chamber at room temperature and atmospheric pressure, $n = 2.5 \times 10^{19}$ molecules/cm³. For vacuum deposition pressures of around 1×10^{-6} torr, there are still 3.2×10^{10} molecules/cm³ remaining. However, this accounts for only 1×10^{-12} of the total volume of the chamber. (4;114)
The molecules of the vapor will travel through the remaining

free space in straight lines until they collide with another molecule or a surface inside the chamber.

As can be seen, the lower the pressure, the less molecules there are in the chamber for the vapor to collide with, and thus the vapor molecules can travel farther between collisions. The mean free path, which is the average distance traveled between collisions with other gas molecules, is dependent on the density and diameter of the gas molecules by: (4;23)

$$L = (\pi\sqrt{2}nd_0^2)^{-1} = \frac{.225}{nd_0^2} \quad (3)$$

where d_0 is the equivalent molecular diameter if a model using hard elastic spheres is assumed. For air at room temperature ($d_0 = 3.7 \times 10^{-8}$ cm),

$$L = \frac{5 \times 10^{-3}}{p} \text{ cm} \quad (4)$$

where p is expressed in torr. From this relationship, it can be seen that for a pressure of 1×10^{-6} torr, the mean free path is 5000 cm. Since in the vacuum system used in this investigation the source to substrate distance is only 60cm, the vapor molecules will travel in straight-line paths and suffer little or no collisions along the way. The fraction of molecules that will or can be expected to experience collisions is given by: (4;115)

$$\frac{N_1}{N_0} = 1 - e^{-r/L} \quad (5)$$

where N_1 is the number of molecules experiencing collisions, N_0 is the original number of molecules, r is the source to substrate distance, and L is the mean free path. For the actual source to substrate distance of 60cm, $r/L = .012$ and 1.19% of the molecules suffer collisions. A very long mean free path, several times the source to substrate distance and achieved by very low pressures, is both useful and desirable.

After the vapor molecules have been emitted from the source and have traveled through the chamber, they arrive at the substrate. Here, the following activities may take place:

(4;124)

- The molecules are "reflected" with most of their original kinetic energy after spending only a short dwell time on the substrate surface.
 - Physical adsorption, in which the vapor molecules are attracted and held mainly by van der Waals forces.
 - Chemical interaction with the substrate material, resulting in a stronger binding of the vapor molecules to the substrate surface.
- or - Association of the vapor molecule to a vapor molecule of the same species already adsorbed on the substrate surface.

The number of molecules that remain on the substrate is described by the vapor's sticking coefficient, which is the fraction of the incident molecules that become strongly bound so that they have a very long dwell time. (4;125) Once on the surface, the molecules may be desorbed, migrate over the surface, or undergo a chemical reaction and become more strongly

bound than it had been after physical adsorption. (4;124)

C. Source Emission and Film Thickness Distribution

When depositing a thin film on a substrate, one is not only concerned with getting the vapor to the substrate and depositing it on the surface, but it is also desired to know how the film will be distributed over this surface. The film's thickness distribution is a characteristic most often considered because it determines the arrangement of source and substrates prior to deposition and how much material will be required. In addition to the physical arrangement of the source and substrate and the amount of material evaporated, thickness distribution depends on the emission characteristics of the sources themselves.

Two of the most common classes of sources, point sources and small plane or surface sources, will be considered. The following assumptions will be made concerning the conditions of the environment in which their emission occurs: (8;143)

- 1) The gas pressure is sufficiently low that collisions between molecules of the vapor and the residual gas (gas remaining after pumpdown) are negligible.
- 2) The intensity of the vapor stream is low enough that collisions between vapor molecules near the emission source are negligible.
- 3) Each vapor molecule reaching the substrate surface sticks upon first impact.

C.1 Point Source. A point source is usually considered as a small emitting sphere that evaporates material equally

in all directions. The geometry of this situation is illustrated in Figure 1.

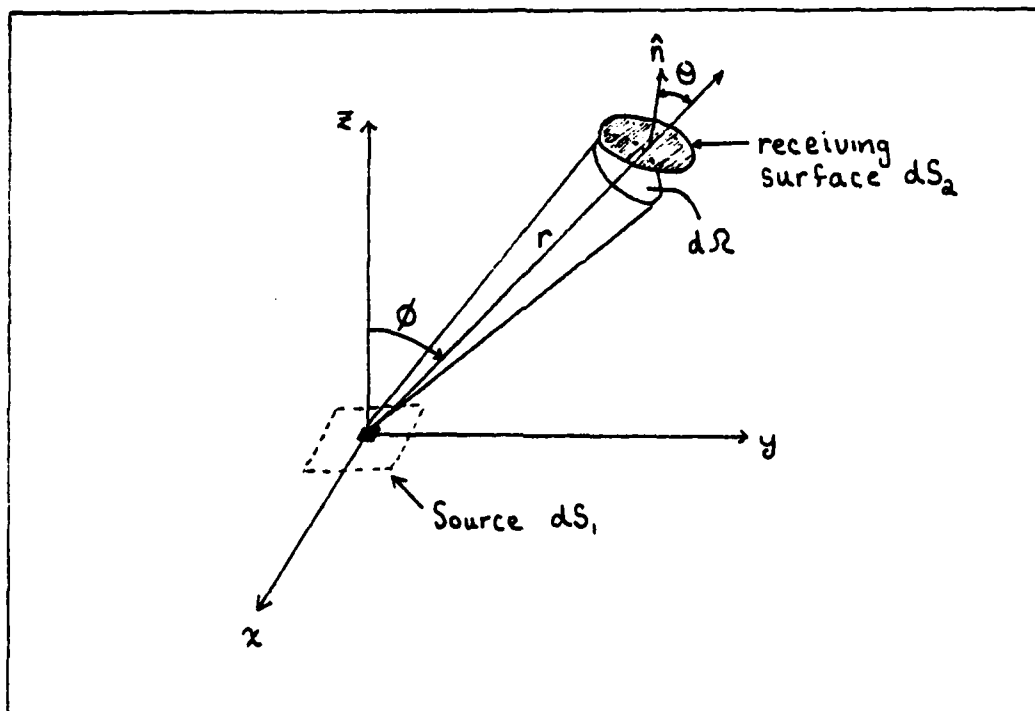


Fig. 1 Evaporation Source Geometry (8;144)

If m_1 is the total amount of mass emitted by the source, the amount of mass dm_2 received at a surface dS_2 will be determined by the amount of material passing through the solid angle $d\Omega$. This results in (4;158)

$$dm_2 = Cm_1 d\Omega = Cm_1 \frac{dS_2 \cos \theta}{r^2} \quad (6)$$

where C is a proportionality constant. To find C , an integration over a spherical receiving surface centered on the source is performed. In this case, $\theta = 0$, $\cos \theta = 1$, and $dS_2 = 2\pi r^2 \sin \phi d\phi$. (4;159)

$$\int dm_2 = \int_{\phi=0}^{\pi} \frac{C m_1 2\pi r^2 \sin \phi d\phi}{r^2}$$

$$m_2 = 4 C m_1 \pi$$

But $m_2 = m_1$, so $C = 1/4\pi$, and

$$dm_2 = \frac{m_1 \cos \theta dS_2}{4\pi r^2} \quad (7)$$

for the mass deposited on the receiving area. If ρ is the density of the deposited mass, the mass can be expressed as the product of the density times the volume. The volume of the deposit is $t \cdot dS_2$, where t is the physical thickness, so (8;144-145)

$$dm_2 = \rho t dS_2$$

and

$$t = \frac{dm_2}{\rho dS_2} = \frac{m_1 \cos \theta}{4\pi \rho r^2} \quad (8)$$

This gives the thickness at specified locations on a surface. To see how the thickness varies over a common deposition surface such as a plane substrate, a calculation using the arrangement in Figure 2 can be done. (8;145) For the case of a point source, $\phi = \theta$ for all angles θ in Figure 2.

The thickness at the point P in the figure is given by (8;146)

$$t = \frac{m_1 \cos \theta}{4\pi \rho r^2} = \frac{m_1 (h/r)}{4\pi \rho (h^2 + r^2)}$$

$$t = \frac{m_1 h}{4\pi \rho (h^2 + x^2)^{3/2}} \quad (9)$$

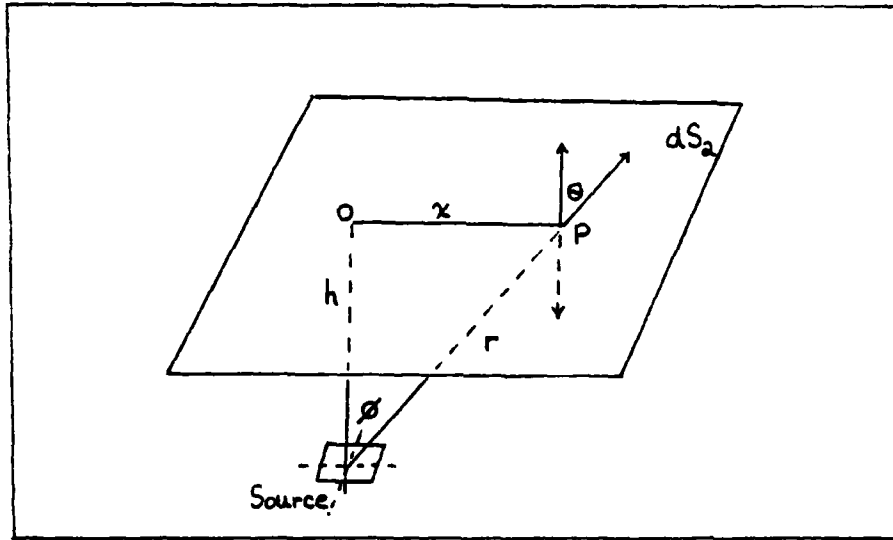


Fig. 2 Evaporation onto a plane substrate (8;145)

The thickness directly opposite the source, at 0, is

$$t_0 = \frac{m_1}{4\pi \rho h^2} \quad (10)$$

since $\cos\theta = 0$ at $x = 0$.

The variation in thickness from the center outward then becomes (8;146)

$$\frac{t}{t_0} = \frac{h^3}{(h^2 + x^2)^{3/2}} = \frac{1}{(1 + (x/h)^2)^{3/2}} \quad (11)$$

C.2 Surface Source. A small plane surface does not emit uniformly in all directions, as does the point source. Instead, Knudsen (9;26-29) has shown that the emission is directional,

depending on the angle between the normal to the source's surface and a line joining the source and the receiving surface. This angle is illustrated as θ in Figure 1. Knudsen's proof of what is known as the cosine law indicates that the amount of material evaporated to a surface in a direction θ from the normal to the source is proportional to $\cos \theta$. (9;26-29, 4;159) The amount of mass received by the surface now becomes (4;160)

$$dm_2 = \frac{Cm_1 dS_a \cos \theta}{r^2} \cos \theta \quad (12)$$

as compared to Eq. (6) for a point source. The constant C is again found by integration over a spherical receiver, but, unlike the point source, the integration is done over a hemisphere, as the surface source emits from one side only, coating only half of the spherical receiver. The result is (4;160)

$$\int dm_2 = \int_{\theta=0}^{\pi/2} \frac{Cm_1 \cos \theta 2\pi r^2 \sin \theta d\theta}{r^2}$$

$$m_2 = Cm_1 2\pi \left[\frac{1}{2} \sin^2 \theta \right]_0^{\pi/2} = Cm_1 \pi$$

Thus $C = 1/\pi$ giving

$$dm_2 = \frac{m_1 \cos \theta \cos \theta dS_a}{\pi r^2} \quad (13)$$

for the mass deposited on the receiving area. The thickness of the deposit on this area is

$$t = \frac{dm_a}{\rho dS_a} = \frac{m_1 \cos \theta \cos \phi}{\rho \pi r^2} \quad (14)$$

As with the point source, Figure 2 can be used to investigate the thickness distribution on a plane substrate placed parallel to the plane source. (8;145) In this orientation, $\phi = \theta$ and the thickness at point P is

$$t = \frac{m_1 \cos^2 \theta}{\rho \pi r^2} = \frac{m_1 (h/r)^2}{\rho \pi (h^2 + x^2)} = \frac{m_1 h^2}{\rho \pi (h^2 + x^2)^2} \quad (15)$$

At 0, the thickness is

$$t_0 = \frac{m_1}{\rho \pi h^2} \quad (16)$$

and the variation in thickness t/t_0 is

$$\frac{t}{t_0} = \frac{h^4}{(h^2 + x^2)^2} = \frac{1}{(1 + (x/h)^2)^2} \quad (17)$$

A plot comparing the thickness variation of the point source, Eq. (11), and the surface source, Eq. (17), is given in Figure 3.

C.3 Obtaining a Uniform Thickness Distribution. Due to the emission characteristics of point and surface sources, it is clear that films deposited on plane substrates will not be uniform unless specific arrangements are made with respect to physical location and orientation of sources and substrates. One such arrangement for small plane sources was made immediately clear in Knudsen's proof of the cosine law. He demonstrated

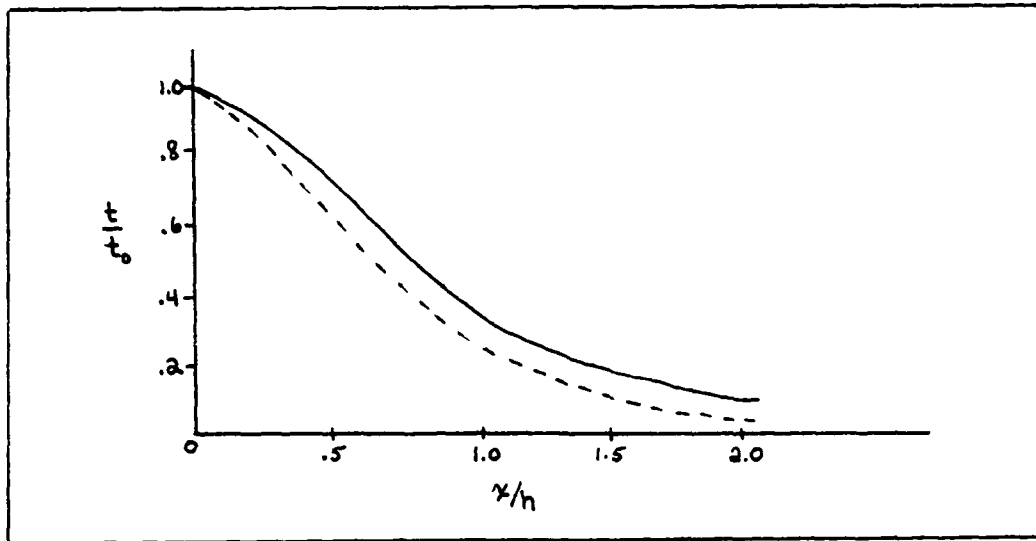


Fig. 3 Thickness Distribution on a Plane Surface
 (8;146, 4;161)
 Solid Line - point source
 Dashed Line - surface source

that if a small plane source emitted from the surface of a sphere, then all other points on that sphere will be uniformly coated. (9;26-29) This can be seen by an analysis of Eq. (14) and Figure 4 below.

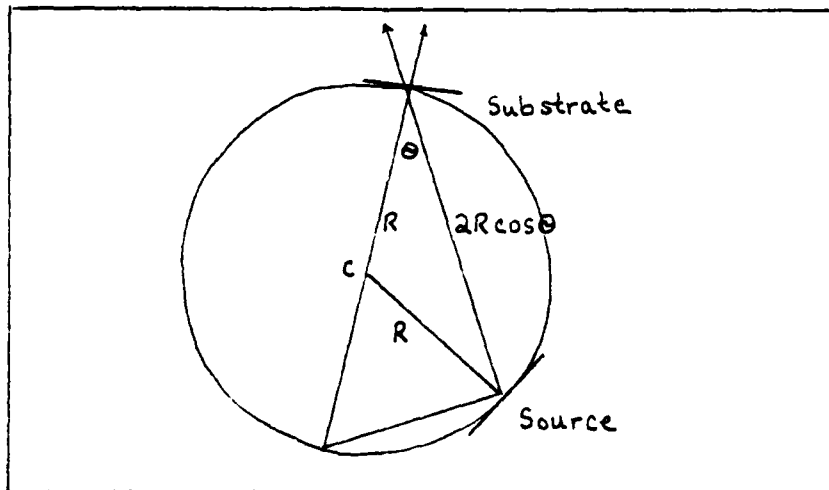


Fig. 4 Arrangement for Knudsen's Proof of the Cosine Law (8,9)

The value for r in Eq. (14), the source to substrate distance, can be seen from Figure 4 to be equal to $2R\cos\Theta$. Substitution of this quantity into Eq. (14) gives

$$t = \frac{m_1}{\rho\pi} \frac{\cos^2\Theta}{4R^2\cos^2\Theta} = \frac{m_1}{4\pi\rho R^2} \quad (18)$$

where R is just the sphere's radius. Since this expression is independent of Θ , the thickness will be determined by the amount and density of the material evaporated. (8;147-148)

For a point source to give a uniform deposit, it should be located at the center of a sphere with the substrates located at points on the sphere. From Eq. (8) then, $\cos\Theta = 1$ and $t = m_1/4\pi\rho R^2$ again for all points on the sphere.

C.4 Application of Emission Characteristics in System Design. The source heater used in the vacuum system for this investigation was an electron beam gun containing a crucible in which the material to be evaporated is placed. Since an open crucible acts like a surface source in its emission characteristics (4;161), an arrangement employing the Knudsen cosine law was designed. The source-to-substrate distance was chosen to be 60cm to make use of the available space within the vacuum chamber. This, of course, made the radius of the sphere in Knudsen's results equal to 30cm. Since a spherical substrate holder of this radius of curvature could not be built, one was designed that approximated a sphere with the substrates being located at the proper distances and orientation for uniform coating to be achieved. The resulting

substrate holder design is illustrated in Figure 5.

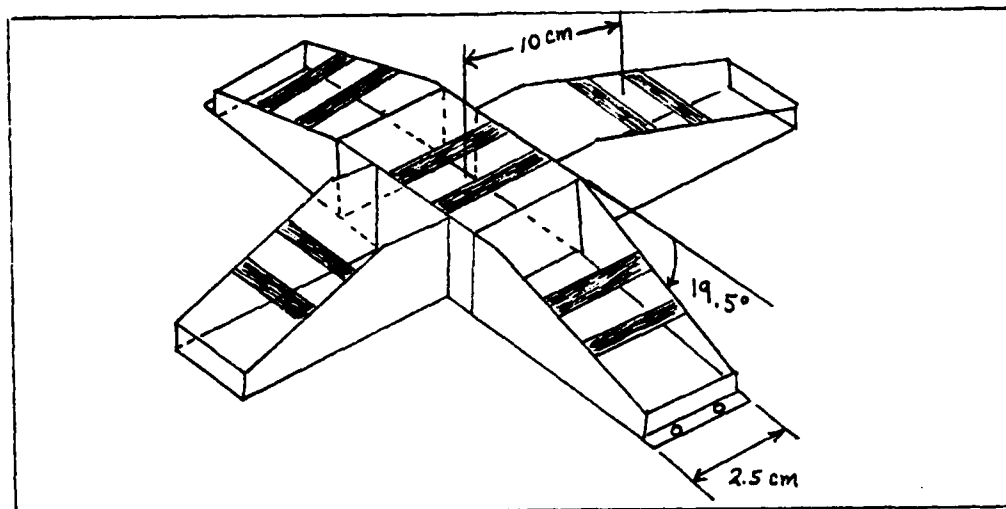


Fig. 5 Substrate Holder

The holder is designed to hold five microscope slides, one at the top center and four others arranged around it. The central substrate will be 60cm from the source and parallel to its surface. The other substrates are located 10cm away from the center of the holder and at an angle of 19.5° from horizontal, thus approximating points on the spherical surface. Actually, in this arrangement, flat microscope slides will only be on the Knudsen sphere at its point of tangency to that sphere. The farther one moves away from this point on the plane surface, the greater the slide will depart from the spherical surface approximation. For the large radius of curvature of this sphere compared to the size of the slides in this case, the approximation should be valid.

III Vacuum Deposition System

A. General

A vacuum deposition system is the apparatus by which thin film optical coatings are produced using the vapor deposition method. The deposition system consists of the vacuum chamber in which the vacuum environment is produced, the source evaporator which produces the vapor to be deposited, and the monitoring system, by which one can control the deposition process and terminate it at the proper time. Obtaining the vacuum environment by the use of a bell jar system will be the main topic of this chapter. A brief description of a source evaporator will also be included.

B. Bell Jar System

The bell jar vacuum system is one type of vacuum system in which a very low pressure environment is produced and maintained so that the vapor deposition process can occur. The system used was the Varian Vacuum Division VI-360 Ultra High Vacuum System. A schematic drawing of this system is shown in Figure 6.

The main components of this vacuum system are five Varian model 941-6001 VacSorb[®] Pumps, a Varian 500 l/sec VacIon[®] Pump, an Hastings model VT-6 thermocouple gauge, and a Varian model 971-0033 Helmer nude ionization gauge. These components will be discussed in the following sections.

B.1 Gas Flow. In order to produce a low pressure environment for conducting thin film deposition, pumps must evacuate

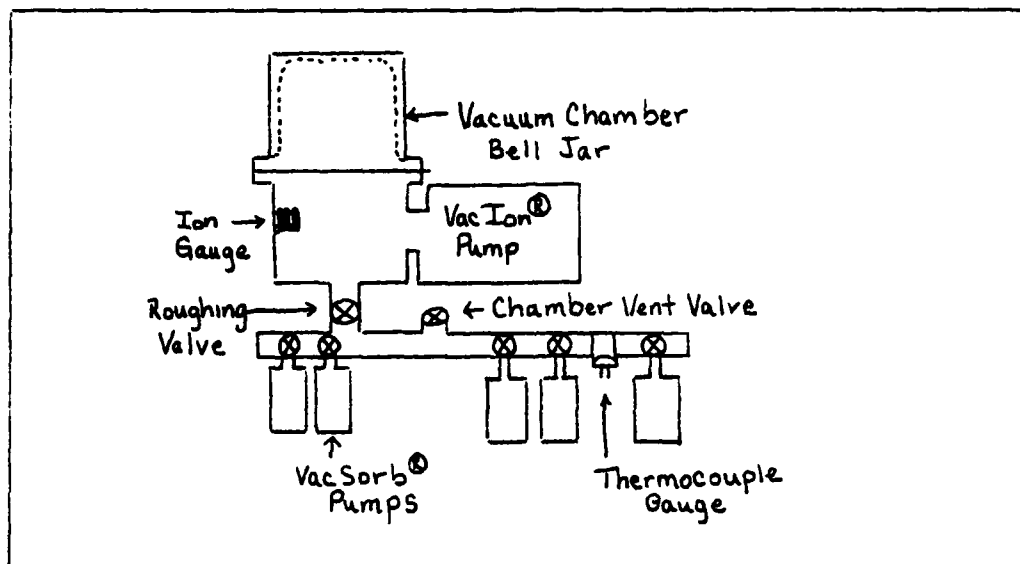


Fig. 6 Bell Jar Vacuum System

gases from a sealed chamber. A number of quantities have been defined (4;31-38) that can be used to characterize the pumps and their removal of gases from the chamber.

The quantity of gas, q , in a certain volume V at pressure p is defined by

$$q = pV \quad (19)$$

and is commonly expressed in units of torr-liters. The time derivative of this quantity is known as the gas flow rate, Q , or throughput. It is defined as

$$Q = \frac{d}{dt}(pV) \quad (20)$$

and measures the quantity of gas which flows across an area per unit time at some specified temperature. Throughput has units of torr-liters/second. If the gas flowing across an area per unit time comes from a container of constant volume, such as a chamber with no leaks or other gas inputs, then it can be seen that $Q = V(dp/dt)$ and throughput is then a measure of

the rate of change of pressure of that fixed volume due to the evacuation of gas.

To get gas to flow across an area or through a section of pipe, there must be a different pressure at one end than there is at the other end. The gas will then flow in the direction of lower pressure. Conductance is a quantity that measures the rate of gas flow (throughput) per unit pressure difference between the two points of interest, i.e.,

$$C = \frac{Q}{p_1 - p_2} \quad (21)$$

where p_1 is the pressure at the entrance and p_2 the pressure at the exit of the object. Conductance has units of liters per second.

Pump speed is defined as

$$S_p = \frac{Q}{p} \quad (22)$$

where p is the pressure at the pump inlet. The definition of pump speed has been used (4;34) to determine a quantity known as the net speed, or exhaust speed, S_E , of the system. This can be expressed as

$$\frac{1}{S_E} = \frac{1}{C} + \frac{1}{S_p} \quad (23)$$

where C is the conductance between the pump and the vacuum chamber and S_p is the pump's speed.

B.2 Roughing Pump. The roughing pumps used in this system are the Varian model 941-6001 VacSorb[®] pumps, one of which is shown in Figure 7. The sorption pump consists of a vacuum-tight cannister containing an adsorbent material. This

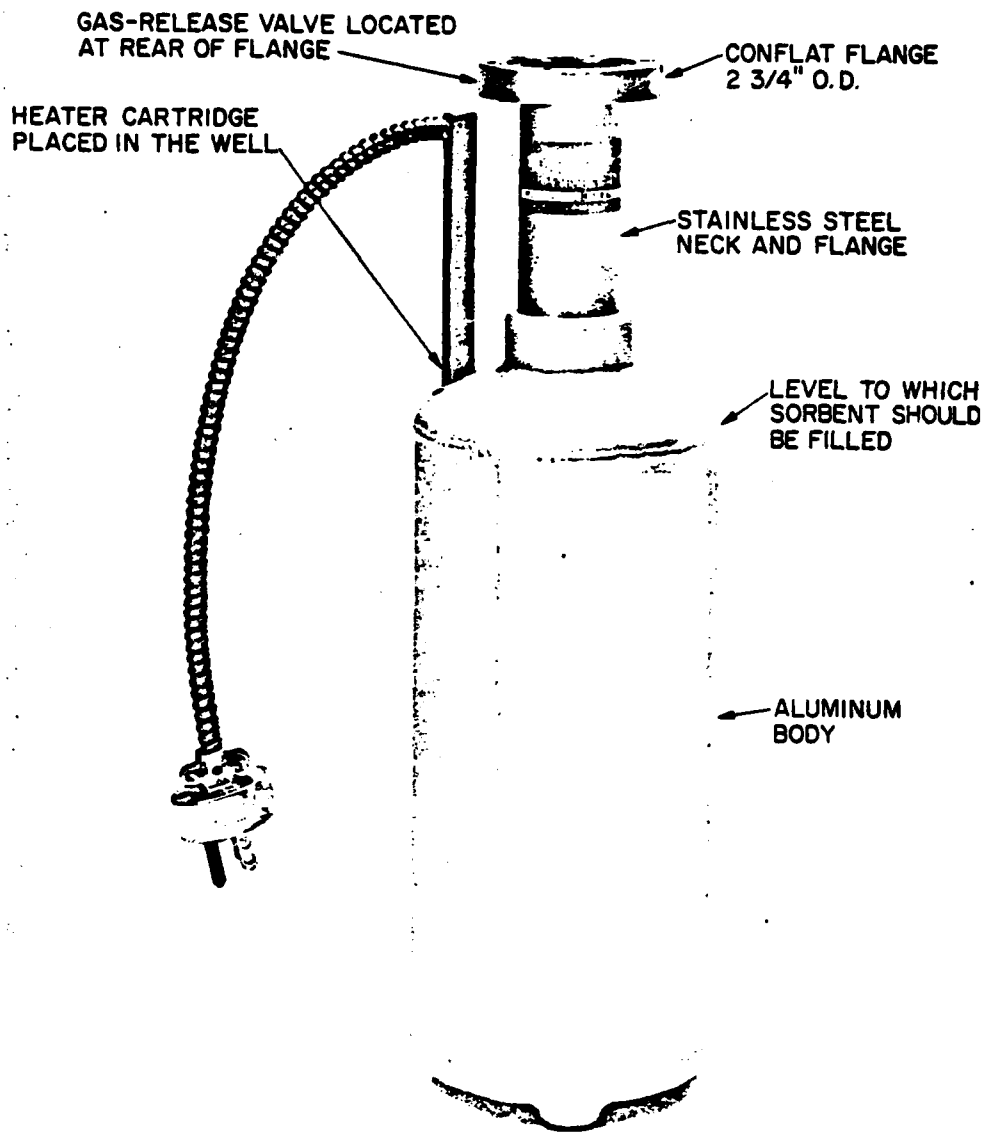


Fig. 7 VacSorb[®] Pump (24)

material provides a surface for a process known as physical adsorption (24;4), in which gases are trapped by being held or adsorbed onto the surface of the adsorbent material by means of van der Waals forces as the gas comes into equilibrium with the surface.

Pumping takes place when the cannister is chilled to liquid nitrogen temperature (-195°C). Since van der Waals forces are also responsible for holding molecules together when a gas condenses, those components of air whose condensation temperature is greater than or equal to that of nitrogen will be drawn from the chamber and adsorbed. The adsorbent material, Type 5A Molecular Sieve manufactured by the Union Carbide Corp., Linde Division, consists of a series of 0.5 nm diameter cavities and pores which are of sufficient size to admit molecules of the various components of air. These cavities and pores increase the surface area on which the gas molecules can be adsorbed. They provide a surface area to volume ratio of $800 \text{ m}^2/\text{cm}^3$; nearly 300 acres of surface area in each VacSorb[®] pump. (24;5)

Due to the size of the pores and the temperature to which the pump is chilled, sorption pumps are rather selective in their adsorption of gases from a vacuum chamber. Since neon and helium liquefy at temperatures lower than that for nitrogen, these gases are hardly pumped at all, leaving a residual atmosphere in the chamber of approximately 70% neon and 7% helium. (24;5) This can be compensated for by using two or more sorption pumps in sequence, depending on the size of the volume to be evacuated. As the first pump is opened to the

system, the inflow of air will also carry helium and neon into the pump, even though they will not be adsorbed. The helium and neon will try to flow back into the system, but as long as there is an inflow of air to the pump, they will be prevented from doing so, being more successful at escaping as the pumping rate slows as the pump nears capacity. Before this occurs, however, the pump can be valved off, trapping the helium and neon permanently, and the remaining pumps can be used in series to complete the pumpdown. (24;16)

Properly used, sorption pumps should be able to evacuate a system to a few millitorr, where a high vacuum pump would be able to take over pumping. Sorption pumps are reactivated by heating to room temperature or above to desorb the trapped gases. Heating well above room temperature is necessary if water vapor has been pumped or is present in the pump. (4;43)

B.3 High Vacuum Pump. The high vacuum pump used was the Varian 500 liter/sec VacIon[®] Pump. This pump is usually operated from 10^{-2} to less than 10^{-11} torr. The pumping element of the VacIon pump consists of several hollow, cylindrical anodes between two titanium cathode plates. One or more of these elements are in turn placed between a strong magnetic field produced by magnets, as illustrated in Figure 8. (25;15)

With an electric field applied, electrons are accelerated from the cathode to the anode, but since the anode is hollow, they pass right through it toward the other cathode where they are repelled back to the anode, setting up an oscillating motion. The magnetic field, oriented parallel to the

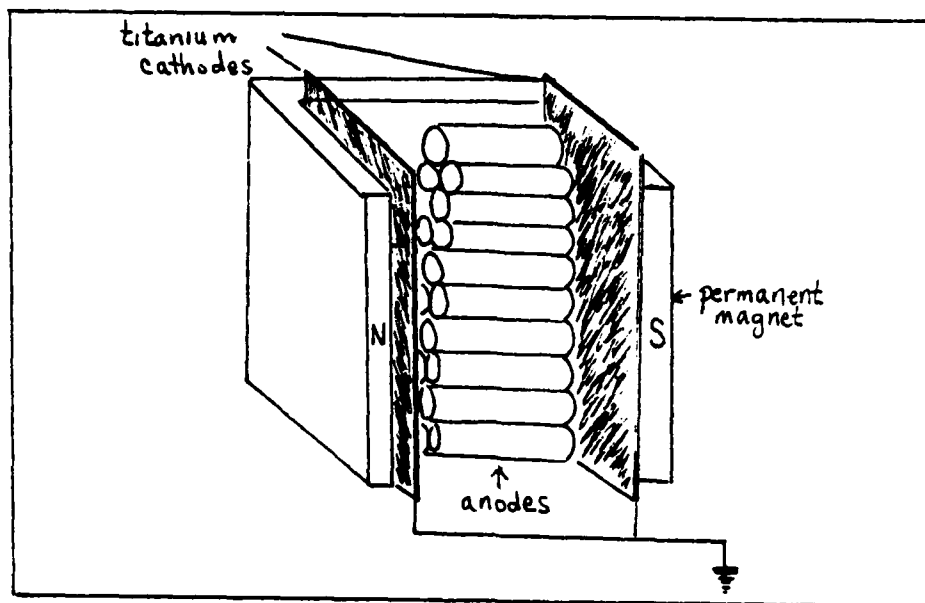


Fig. 8 VacIon® pumping element (25;15)

electronic oscillations, causes the electrons to move in a spiral, lengthening the path of their movement. This increases the probability of an electron colliding with an atom or a molecule, producing ions and more electrons. The electrons help to maintain the discharge while the positive ions from the gas bombard and become embedded in the cathode, sputtering titanium in the process. (25;16, 4;53)

The sputtered titanium atoms are deposited on the anode and on other surfaces inside the pump, forming a fresh getter surface. A getter is some material that will remove gases by sorption, discussed earlier. (4;53) The titanium will react with active gases such as nitrogen and oxygen to form stable compounds and remove these gases from the chamber. These gases may also combine with the titanium in the cathodes, but may be resputtered (decomposed or intact), or they can even

penetrate the cathode up to a few atomic layers and become trapped through ion burial. (25;17-18)

Ion burial is the main process by which inert gases are pumped. Once ionized, these gases penetrate and become embedded in the cathodes. However, as the cathode becomes eroded by further ion bombardment, these ions and any others trapped can be reemitted, making the ion pump somewhat inefficient for inert gases. The titanium getter surface, on the other hand, is the main process for active gas removal. (4;54)

B.4 Vacuum Gauges. As the various pumps were operating through their respective regions, it was necessary to monitor the pressure in the system in order to insure that adequate pumping was being accomplished and to locate the proper pressure to start or stop a certain type of pump. Unexpected rises in the pressure may be used to signal problems such as leaks or outgassing. The two major types of vacuum gauges used to measure the pressure were the Hastings model VT-6 thermocouple gauge and the Varian model 971-0033 Helmer ionization gauge. Both of these gauges are effective only in certain pressure ranges and must be used in combination for full scale monitoring to be possible.

The thermocouple gauge is used mainly from atmospheric pressure down to 1 millitorr, although it is more accurate when used in the range 10^{-3} - 1 torr. The accuracy of this gauge is given as 2% of fullscale angular meter deflection. (26) The gauge is designed on the principle that the thermal conductivity of a gas is dependent on the gas pressure.

The thermocouple gauge consists of a heated filament located inside a tube, with the filament in contact with a thermocouple. The thermocouple measures the temperature of the heater and thus gives a measure of the amount of heat being conducted away from the filament to the tube wall by the gas. As the pressure falls, there are less molecules available to transport heat, conduction falls, and the filament becomes hotter. This temperature rise is detected by the thermocouple and its output current is increased, which shows as a needle deflection on the tube gauge. (26, 4;82)

For pressures below 10^{-3} torr, the ionization gauge is used. Basically, an ionization gauge uses electrons, usually produced by thermionic emission from a hot filament, to ionize gas molecules in the vicinity of the gauge. The ions produced are collected on a cathode and measured as a current. Since the ion current is proportional to the number density of molecules available to be ionized, this is used as a means of measuring pressure. (4;85)

The Helmer Ionization Gauge is a nude ionization gauge which can be used in the 10^{-4} to 10^{-13} pressure range. (27) "Nude" gauges are ones that have their elements in the vacuum chamber rather than in a separate tube connected to it.

C. Electron Gun Source

A device called an electron gun is used to evaporate a source by heating it with high energy electrons. The electron gun used in this system is the Varian model 980-0003 e-GunTM Source. Its principle of operation is illustrated in Figure 9.

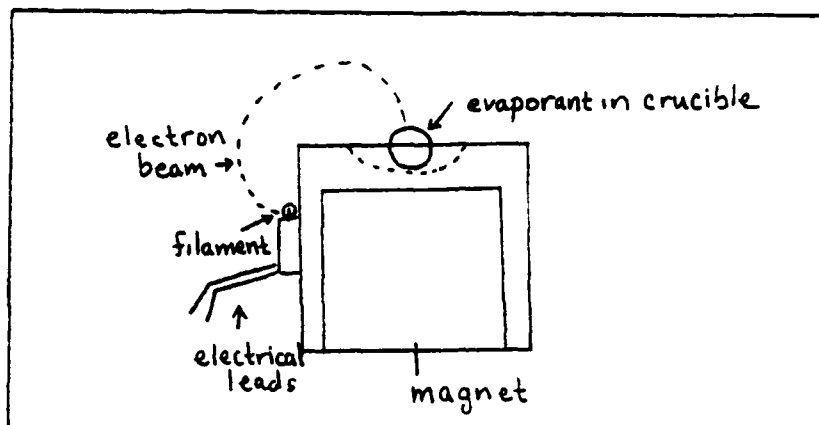


Fig. 9 Electron Beam Gun

Electrons are emitted by a hot-filament tungsten cathode, accelerated by a separate anode (self-accelerated source), and focused by a magnet so that the electron beam falls directly on the evaporant source resting in a water-cooled crucible. In work-accelerated sources, the evaporant is the only anode. (4;140) The beam is bent 210° in the Varian e-Gun, allowing the evaporant/crucible to be located such that it is shielded from contamination by the hot filament emissions. Focusing the electron beam to strike only the evaporant also prevents contamination. In addition, the heat for evaporation is generated in the evaporant and not the crucible, providing more efficient heating and less heat radiated from the overall source. Water cooling the crucible helps prevent the evaporant from interacting with its holder and guards against the holder material being evaporated along with the evaporant. (28, 4;139) The Varian e-Gun can operate at pressures below 5×10^{-4} torr, requires only .5 gal/min cooling water flow, has a maximum power output of 2kW, and a beam intensity of 25 kW/cm^2 . (28)

Even with all the advantages of electron gun use, there are a few disadvantages to be noted. The source is more complicated than resistance heated sources; compounds can be partially dissociated by the electron beam; and the portion of the evaporant vapor that has to pass through the beam, plus any residual gas molecules present, may become ionized.

(4;139-140)

IV Optical Monitoring of Film Thickness

In addition to having the proper environment for thin film evaporation to occur, and having a source and substrate oriented to take advantage of the particular emission characteristics of the source, one also needs to be able to monitor the deposition process, preferably while it is taking place, in order to make films of the desired thickness. This chapter discusses one of the means by which this can be done, known as the optical monitoring technique.

An optical film thickness monitor consists of a light source illuminating a test substrate and detectors to receive and measure the transmitted and/or reflected light. Once the desired optical properties are achieved, the vapor source can be turned off and the deposition stopped.

The quantity determined by the optical technique is the film's optical thickness. Optical thickness is defined as the product of the film's index of refraction and its physical thickness. The optical thickness of a thin film has certain characteristic properties when its value is an integral multiple of a quarter wave. These properties, used in determining the film's thickness, are presented in the following sections.

A. Theory - Quarter Wave Films

In the following discussion it is assumed that light is incident normally on the film-substrate combination and that there are no losses due to absorption. Each layer of film deposited can be represented by the characteristic matrix (18;5),

developed in Appendix A:

$$\begin{bmatrix} \cos \delta_j & \frac{i \sin \delta_j}{N_j} \\ i N_j \sin \delta_j & \cos \delta_j \end{bmatrix} \quad (24)$$

where δ_j is the phase thickness of the j^{th} layer, given by

$$\delta_j = \frac{2\pi N_j d_j}{\lambda} \quad (25)$$

where N_j is the index of refraction of the layer and d_j is the physical thickness of the layer. The optical thickness of the layer is expressed as $D_j = N_j d_j$ and is most commonly given in terms of fractional wavelengths (i.e., $\lambda/4$ for a quarter wave).

A term that is related to the index of refraction of a thin film and is often used in the determination of its optical properties is optical admittance. Optical admittance is defined by $Y = Y_0 n$, where n is the index of refraction and Y_0 is the admittance of free space. Y_0 is equal to one in Gaussian units and 1/377 siemens in SI units. (17;7) Numerically, optical admittance is calculated as the ratio of the magnitudes of the magnetic and electric fields of a wave, H/E , such as that from the monitor's light source. (17;7) H and E for a multilayer film are determined by (18;5)

$$\begin{bmatrix} E \\ H \end{bmatrix} = \left\{ \prod_{j=1}^m \begin{bmatrix} \cos \delta_j & \frac{i \sin \delta_j}{N_j} \\ i N_j \sin \delta_j & \cos \delta_j \end{bmatrix} \right\} \begin{bmatrix} 1 \\ n_{\text{sub}} \end{bmatrix} \quad (26)$$

where m is the number of layers making up the multilayer film, and n_{sub} is the index of refraction of the substrate.

Since the admittance determined by E and H is proportional to the effective refractive index for the film-substrate combination, the Y_0 factor will drop out when the admittance is used in place of the refractive index in the Fresnel equation for reflectance at normal incidence. This will give for the reflectance of the multilayer at normal incidence:
(18;5)

$$R = \left| \frac{1-Y}{1+Y} \right|^2 \quad (27)$$

where Y is the optical admittance defined earlier. This definition, plus Eqs. (26) and (27), implies that the reflectance of the multilayer film at any point during its production can be considered as being produced by a film-substrate combination of an effective index proportional to Y , determined by the material deposited up to that point. Also, subsequent material for the next layer will act as if it were being deposited on a substrate of index proportional to Y , as if the already deposited film and substrate were one material of index proportional to Y . (18;5)

Since the admittance changes continually during the deposition process, plotting its locus for the entire deposition gives an indication of how the index of refraction of the combination changes and also how the reflectance changes during the process. Y will be calculated using the characteristic matrix

$$\begin{bmatrix} E \\ H \end{bmatrix} = \begin{bmatrix} \cos \delta & \frac{i \sin \delta}{N} \\ i N \sin \delta & \cos \delta \end{bmatrix} \begin{bmatrix} 1 \\ \alpha + i\beta \end{bmatrix} \quad (28)$$

where $Y = H/E$ is the admittance and $\alpha + i\beta$ is the admittance of the material deposited so far. $\alpha + i\beta$ can also be considered the index of the existing film-substrate combination, which will then act as the substrate for the next layer. δ is the phase thickness, defined earlier, for the layer being deposited and N is its refractive index. (18;6) Y will generally be complex and will be equal to

$$Y = a + ib = \frac{\alpha \cos \delta + i(N \sin \delta + \beta \cos \delta)}{(\cos \delta - \frac{\beta \sin \delta}{N}) + \frac{i \alpha \sin \delta}{N}} \quad (29)$$

This will then result in

$$\begin{aligned} a \cos \delta - \frac{a\beta \sin \delta}{N} - \frac{\alpha b \sin \delta}{N} + i \left(b \cos \delta - \frac{b\beta \sin \delta}{N} + \frac{a\alpha \sin \delta}{N} \right) \\ = \alpha \cos \delta + i(N \sin \delta + \beta \cos \delta) \end{aligned}$$

Equating real and imaginary parts gives (18;6, 17;30)

$$\left. \begin{aligned} a \left(\cos \delta - \frac{\beta}{N} \sin \delta \right) - \frac{\alpha b}{N} \sin \delta &= \alpha \cos \delta \\ b \left(\cos \delta - \frac{\beta}{N} \sin \delta \right) + \frac{a\alpha}{N} \sin \delta &= N \sin \delta + \beta \cos \delta \end{aligned} \right\} \quad (30)$$

To eliminate δ from the equations, Eqs. (30) are rewritten in the following form:

$$\left(-\frac{a\beta}{N} - \frac{\alpha b}{N}\right) \sin \delta = (\alpha - a) \cos \delta \quad (31a)$$

$$\left(\frac{a\alpha}{N} - \frac{b\beta}{N} - N\right) \sin \delta = (\beta - b) \cos \delta \quad (31b)$$

Solving (31a) for $\cos \delta$ and simplifying after substitution into (31b) gives

$$a^2 + b^2 - a\left(\frac{\alpha^2 + \beta^2 + N^2}{\alpha}\right) + N^2 = 0 \quad (32)$$

Thus, the admittance locus is, as seen by Eq.(32), a circle with center (18;6, 17;30)

$$\left(\frac{\alpha^2 + \beta^2 + N^2}{2\alpha}, 0\right) \quad (33)$$

Since $\alpha + i\beta$ is the substrate index, and β is related to the extinction coefficient which determines the loss due to absorption effects, for no absorption $\beta = 0$, $n_{\text{sub}} = \alpha$ and Eq. (33) can be rewritten:

$$\left(\frac{n_{\text{sub}}^2 + N^2}{2n_{\text{sub}}}, 0\right) \quad (34)$$

The admittance locus can be plotted on an Argand diagram as shown in Figure 10. (18;6) Since deposition starts on a substrate with n_{sub} , $(\alpha, 0)$ is the starting point for the circle, which is traced out in a clockwise direction.

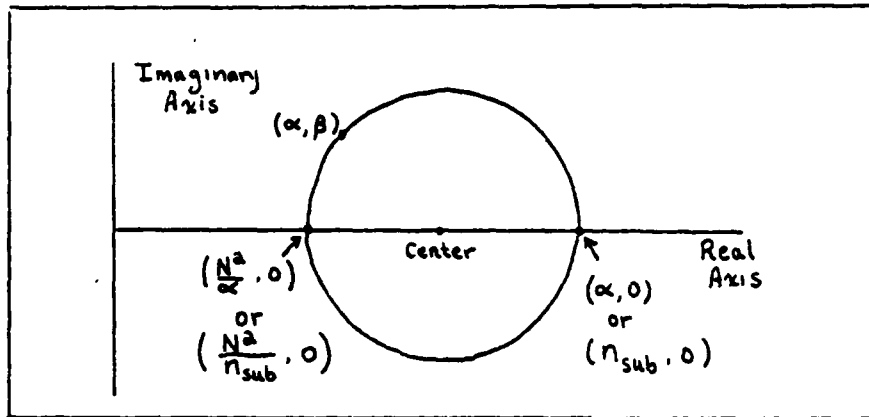


Fig. 10 The Admittance Locus (18;6)

To plot loci of constant δ on the diagram for a film of index N , β is set equal to zero in Eq. (30) giving (18;6, 17; 30)

$$\left. \begin{aligned} a \cos \delta - \frac{\alpha b}{N} \sin \delta &= \alpha \cos \delta \\ b \cos \delta + \frac{a \alpha}{N} \sin \delta &= N \sin \delta \end{aligned} \right\} \quad (35)$$

or,

$$a - \frac{\alpha b}{N} \tan \delta = \alpha \quad (36a)$$

$$b + \frac{a \alpha}{N} \tan \delta = N \tan \delta \quad (36b)$$

Eliminating α by solving Eq. (36b) for α and substituting the result into Eq. (36a) and then simplifying gives:

$$a^2 + b^2 + bN \left(\frac{1}{\tan \delta} - \tan \delta \right) - N^2 = 0 \quad (37)$$

Equation (37) is a circle with its center at

$$\left(0, \frac{N}{2} \left(-\frac{1}{\tan \delta} + \tan \delta \right) \right) \quad (38)$$

which is on the imaginary axis of Figure 10. The equations described by (37) all pass through the point $(N,0)$, as can be seen if $b = 0$ for the $a + ib$ system of Figure 10.

The result of plotting two simple cases of Eq. (37) onto Figure 10 is shown in Figure 11. (18;7)

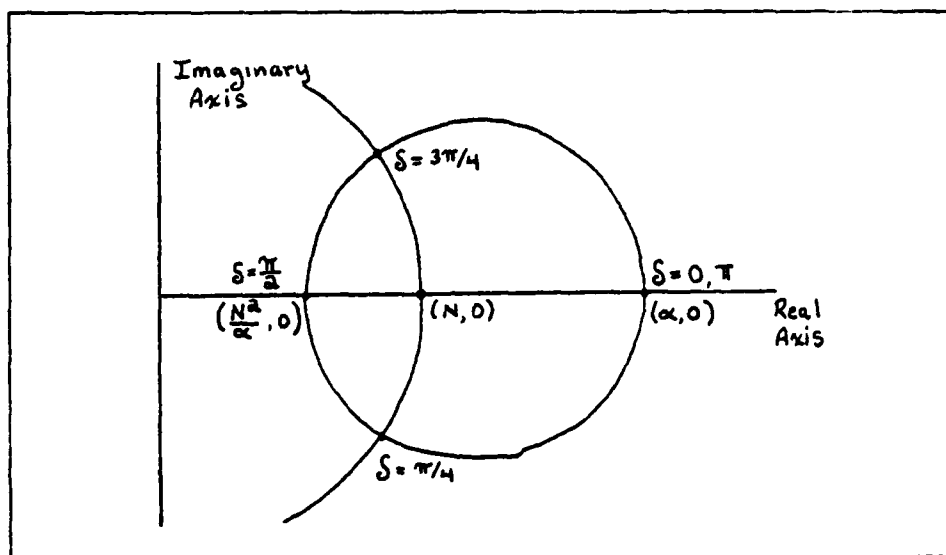


Fig. 11 Admittance Diagram with constant δ contours added (18;7)

If $\delta = 0, \pi/2, \pi, 3\pi/2, \dots$ the result is the real axis. However, if $\delta = \pi/4, 3\pi/4, 5\pi/4, \dots$ the result is the circle shown in Figure 11 with center at the origin and passing through the point $(N,0)$. (18;7)

Using Eq. (25), the definition of the phase thickness, one can correlate the values for δ shown in Figure 11 to optical thickness, $N \cdot d$. Thus, $0 \rightarrow 0, \pi/4 \rightarrow \lambda/8, \pi/2 \rightarrow \lambda/4, 3\pi/4 \rightarrow 3\lambda/8, \pi \rightarrow \lambda/2, \dots$ so that as the circle is traced, the optical thickness increases from zero at the starting point on the real axis to $\lambda/4$ where it again intersects the real axis,

and $\lambda/2$ when the circle is completed. Thus each full circle represents a half wave layer of index N material.

Isorefectance contours can also be constructed on the same diagram to indicate how changes in layer thickness affect the reflectance of the film. The contours are developed in the following manner:

The Fresnel reflectance equation is

$$R = \left(\frac{n_{\text{eff}} - 1}{n_{\text{eff}} + 1} \right)^2 \quad (39)$$

where n_{eff} is the effective index of refraction of the film-substrate combination. Since the admittance of the combination is proportional to n_{eff} , and of the form $a + ib$, the reflectance can be represented as

$$R = \left(\frac{a + ib - 1}{a + ib + 1} \right)^2 = \left(\frac{(a-1) + ib}{(a+1) + ib} \right)^2 = \frac{(a-1)^2 + b^2}{(a+1)^2 + b^2} \quad (40)$$

which will then give

$$a^2 + b^2 - 2a \frac{(1+R)}{(1-R)} + 1 = 0 \quad (41)$$

This represents a circle centered on the real axis with center (18;7, 17;31)

$$\left(\frac{1+R}{1-R}, 0 \right) \quad (42)$$

The radii of the various isorefectance curves can be related to a given value of reflectance by the following relationship: (23;296)

$$r = \sqrt{d^2 + e^2 - f} \quad (43)$$

where the variables come from the general form for a circle:

$$x^2 + y^2 + 2dx + 2ey + f = 0 \quad (44)$$

Substituting the known values from Eq. (41) into (43),

$$r = \sqrt{\frac{(1+R)^2}{(1-R)^2} - 1} = \frac{2\sqrt{R}}{1-R} \quad (45)$$

When the isorefectance curves are added to the admittance diagram, the result is as shown in Figure 12. (17;32)

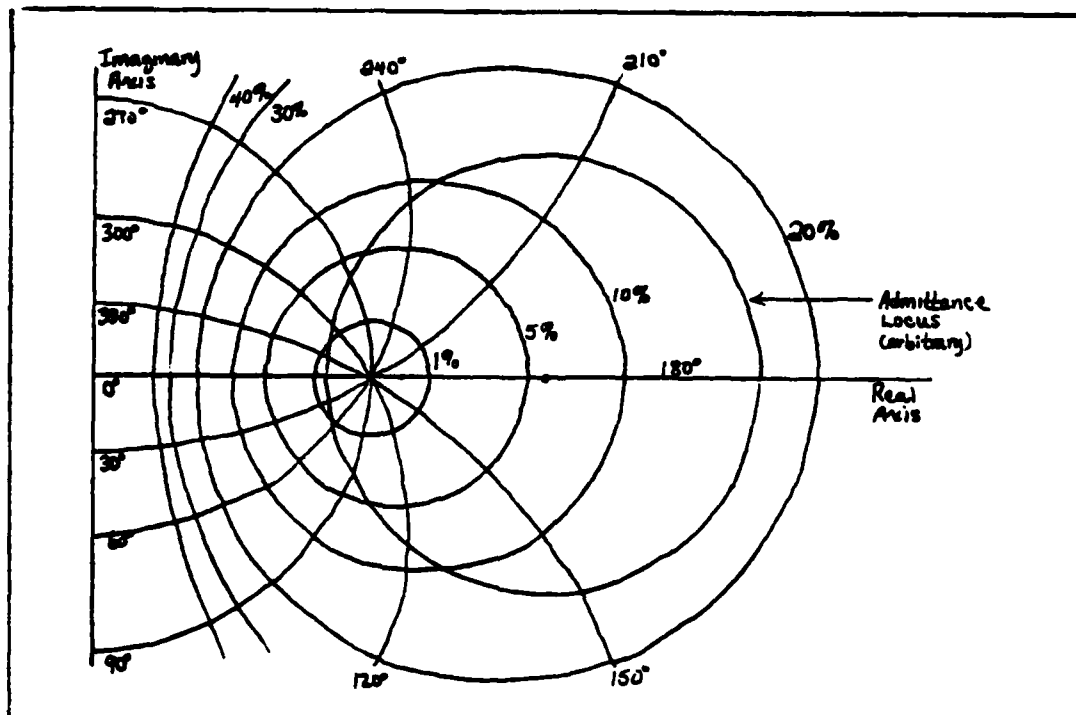


Fig. 12 Admittance locus with constant S contours and isorefectance contours added (17;32)

As can be seen from Figure 12, as the admittance curve is traced from thicknesses of 0 to $\lambda/4$ to $\lambda/2$ and higher, the reflectance of the film will cycle periodically between some peak value and the reflectance of the bare substrate at the start of deposition. These turning values of reflectance correspond with the intersections of the admittance locus with the real axis, since both curves have their centers on that axis. (18;8) This ideal case is represented in the curves of Figure 13. Note that the peak value of reflectance achieved is dependent on the index of refraction of the material deposited, in accordance with the Fresnel equation.

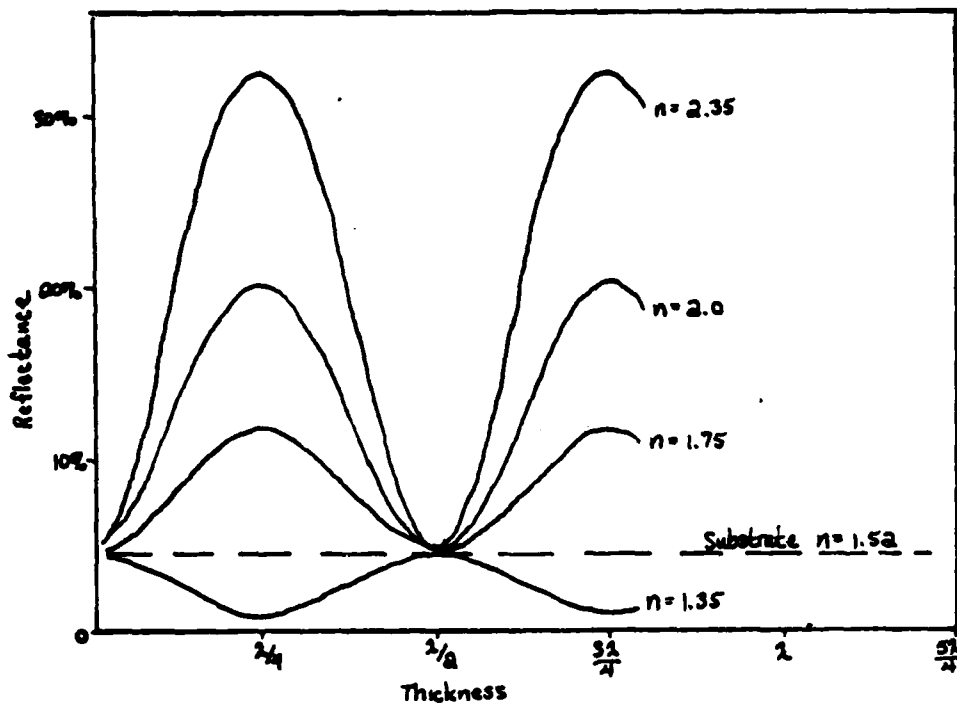


Fig. 13 Variation of Reflectance with Film Thickness (16;235)

These characteristic turning values for layers of quarter-wave thickness can then be used in the deposition process as a monitoring and control technique. For desired deposition of a quarter wave layer of some material of index N , one needs to monitor the light reflected or transmitted (since for lossless media, i.e., absorption equal to zero, $T = 1 - R$) at a certain wavelength for the appearance of a turning value in R or T which indicates that a quarter-wave-thick film has just been deposited. For layers of an integral number of quarter waves in thickness, one needs only to count the turning points observed until the desired number of quarter wave thicknesses have been deposited.

The technique of turning value monitoring can be carried out in a few different ways. (14;383-4, 12;85) One method, known as direct monitoring, has all the layers of a multi-layer film monitored directly on one of the substrates to be used after coating. Indirect monitoring is a method by which each layer is monitored on a separate test substrate. A third method, semi-direct monitoring, has all the layers of the film deposited and monitored on the same test substrate, but separate from the ones to be produced for eventual use. Direct monitoring has the advantages that the deposit being monitored will be what will actually be produced, and of the effects of a powerful error compensation process. The main effect of this process is that an error in the thickness of one layer can be compensated for by the way in which the next layer is deposited. A more detailed explanation and analysis of this process can be found in references 13, 15, and 18.

When separate test substrates are used for each layer in the indirect process, each layer can be monitored separately so that an error in one layer will not affect all the subsequent layers of the film. Also, a possible loss of the monitor signal, caused when the reflectance becomes too high while depositing certain types of coatings, can be avoided. However, differences in the condensation, or "sticking", effects between materials that are deposited on the film surface they were intended to be evaporated onto vs. that for the bare substrate (of different index than the combination produced to that point) may adversely affect the final result. Semi-direct monitoring retains the advantages of direct monitoring and avoids the sticking difference problem of indirect monitoring. Any differences in index between the test substrate and those intended for actual production that are small can be compensated for by precoating the test substrate in order to increase the monitoring signal's magnitude. (14;384)

B. Absorption Effects

In the ideal case, a film deposited on a substrate will produce a regular, repeating sinusoidal curve that is bounded by a maximum and a minimum value of transmittance, as was illustrated in Figure 13. These maximum and minimum values, in the ideal case, remain constant and the transmittance curve alternates between a maximum turning point and a minimum turning point with every quarter wave thickness of film deposited. This can also be seen from the admittance locus of Figure 10, where the circle would be traced repeatedly, a quarter wave

being deposited with every crossing of the real axis, clearly indicating that the turning values would alternate between some fixed maximum and minimum values.

An actual film would not behave in this manner since absorption, though small, does have an effect on the resulting reflectance and transmittance after each layer is deposited. The following analysis by Macleod (11;500-1) shows how absorption can affect the performance of the layer.

If a quarter wave layer of index $n - ik$ ($k \neq 0$ in the case where absorption is present) is deposited on a substrate of real index N , the effective admittance of the combination is found using $Y = H/E$, where H and E are now determined by (11;500)

$$\begin{bmatrix} E \\ H \end{bmatrix} = \begin{bmatrix} \cos \delta & \frac{i \sin \delta}{n - ik} \\ i(n - ik) \sin \delta & \cos \delta \end{bmatrix} \begin{bmatrix} 1 \\ N \end{bmatrix} \quad (46)$$

δ is the phase thickness of the layer and is determined by (11;501)

$$\begin{aligned} \delta &= \frac{2\pi}{\lambda} (n - ik) d \\ &= \frac{2\pi}{\lambda} (1 - i(k/n)) D \end{aligned} \quad (47)$$

where D is the optical thickness, d is the physical thickness, and λ is the monitoring wavelength. Macleod's analysis produces for the error in admittance away from ideal due to absorption as

$$\frac{\Delta Y}{Y} = \left(\frac{N}{n} - \frac{n}{N} \right) \alpha \quad (48)$$

where α is defined as $\pi k/2n$. (11;501) This effect on admittance is similar to the shift caused by errors in terminating layer deposition properly at the turning value. (11;502, see also ref 18) This would thus only result in a shift in final reflectance after each layer is deposited away somewhat from the ideal case described at the beginning of this section. The reflectances at the turning points, rather than always coming back to the same maximum and minimum values, will tend to turn at slightly higher maximum and minimum values each time, giving a general trend toward unity as more layers are added, and the variable part of the signal will become gradually smaller compared to the total signal as the maximum and minimum turning values approach each other. (16;237) For transmission monitoring, the variable part of the signal remains a large part of the overall signal, but the trend here is for the signal to go toward zero, where after a certain number of layers dependent on the quality of the system used for the monitoring, the signal will get lost in the noise from the system. (16;237-8) An example of the zero-ward trend of the transmission signal with continued deposition of quarter wave layers can be seen in Figure 14.

C. Changes in Films Due to Packing of the Deposit and Moisture Absorption

Two processes that can affect the film's performance during and after film deposition in spite of the accuracy of monitoring achieved involve how the individual atoms or molecules build up a film on the substrate surface, packing; and

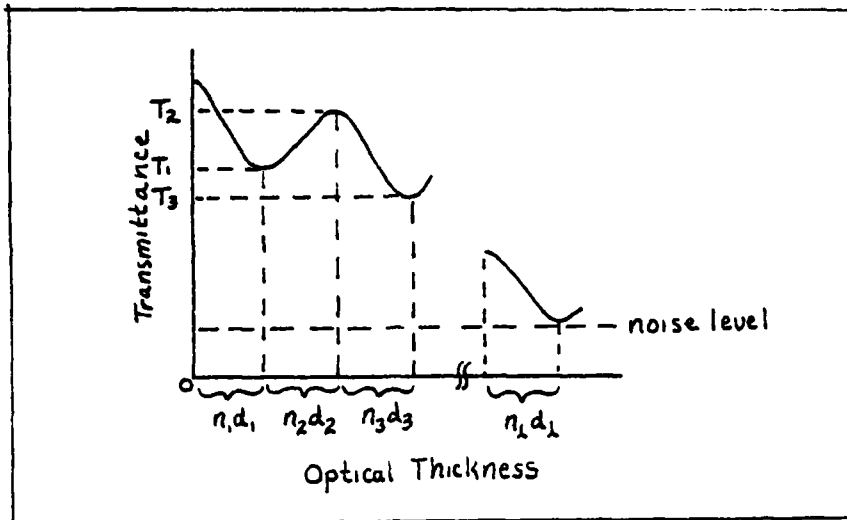


Fig. 14 Trend of Transmission Signal
Toward Zero for Many-Layered
Deposition (5;169)

the potential for moisture absorption by the film after it has been deposited. These processes can affect the actual monitoring of the film during deposition by altering the film's index of refraction, producing a film of optical thickness that may differ from what was intended, or they may alter the final performance of the completed film to an unintended wavelength range.

The packing of the atoms or molecules in the deposit is determined by how they condense and adhere to the substrate surface and each other. Most of the dielectric materials deposited as thin films are believed to build in a columnar structure. (14;387) If the atoms are thought of as hard spheres, the columns would be circular in cross section so that even with the closest packing arrangement possible there would still be empty spaces between the columns. This empty space will tend to reduce the density and the index of refraction

of the film as a whole. (14;387) Packing density is defined as the ratio of the volume of the solid material in the film to the total volume available in the film (solid plus the voids - its geometrical volume) so that a packing density of .85 would indicate that 15% of the film's volume is empty space. The packing density can be used to determine the index of refraction of the film after such space is taken into consideration using (14;388)

$$n_f = pn_o + (1-p)n_p \quad (49)$$

where n_f is the resulting index for the film, p is the packing density, n_o is the index of the solid part of the film (the material deposited), and n_p is the index of the spaces in the film (usually equal to one). This equation does reasonably well to estimate the effect that packing density has on the film's index for deposited materials of low index of refraction or very high values of refractive index. For intermediate values, a more complicated expression is necessary to describe this effect.

Since the optical thickness of a film is determined by $n_f d$, where d is the film's physical thickness, the effect packing density has on optical thickness through the index of refraction is (14;388)

$$D_f = \left\{ 1 + \frac{(1-p)n_p}{pn_o} \right\} D_o \quad (50)$$

where D_o is the optical thickness the film would have if it were completely solid.

The other process affecting the film's performance and due to the porosity caused by the columnar structure mentioned earlier is the absorption of moisture by the film. When exposed to atmospheric air, the spaces between solid material allow moisture from the air to enter the film. The moisture penetrates the film in the following manner: (15;341) Moisture enters the film rapidly upon exposure to air and the absorption may continue for a number of days. The outermost layer of the film is affected first, and after this layer is saturated the moisture spreads to lower layers in sequence. The moisture does not enter a particular layer uniformly, depending mainly on the sizes of the spaces available between solid material, affecting the film unevenly over its surface.

The resulting effect of the absorption of moisture by a film is for the index of the spaces between columns to increase, increasing the index for the entire film as seen by Eq. (49), and leading to a larger optical thickness for the layers affected. (15;340) Due to the resulting increase in optical thickness caused by moisture absorption, the optical characteristics of the film will tend to shift from the wavelength used in the monitoring of the film toward longer wavelengths. (14;389) To reduce this effect where thermal evaporation is the desired deposition process, it is suggested (15;341) that a cover glass be cemented over the film immediately after production and that the edges of the film be sealed also, as moisture can enter from the edges as well. It should be noted that this procedure, rather than completely stopping the absorption of moisture, may in most cases only slow it down. (15;341)

V Quartz Crystal Monitoring

A. Theory and Operation

One of the most common non-optical methods for thickness monitoring during film deposition is the quartz crystal oscillator. This system consists of a vibrating quartz crystal mounted inside the vacuum chamber and exposed to the evaporant stream in such a way that it receives the same coating as the production substrates. As the quartz crystal is coated, the change in its vibrational frequency is measured to determine the mass of the deposit. From this mass, the thickness of the film deposited may be determined.

Change of mass, however, is not the only factor that may affect the resonant frequency of the quartz crystal. Changes in temperature affect frequency through the temperature coefficient of frequency (TCF) which is related to its various elastic constants. (3;24, 19;1--108) The TCF has terms that are positive and negative, the magnitudes of which depend on the direction of the vibration with respect to the natural axes of the crystal. (19;1--108) Since changes in frequency due to temperature changes will have an effect on the accuracy of the measurements of deposited mass, it is desirable to reduce the magnitude of the TCF as much as possible. There is a certain cut of the quartz crystal, shown in Figure 15 and known as the AT-cut, where the terms in the TCF are found to balance each other and minimize the overall magnitude of the TCF. (19;1--108) With a cut of $35^{\circ}20'$, the temperature coefficient remains below $5 \times 10^{-6} \text{ deg}^{-1}$ between about -5°C and

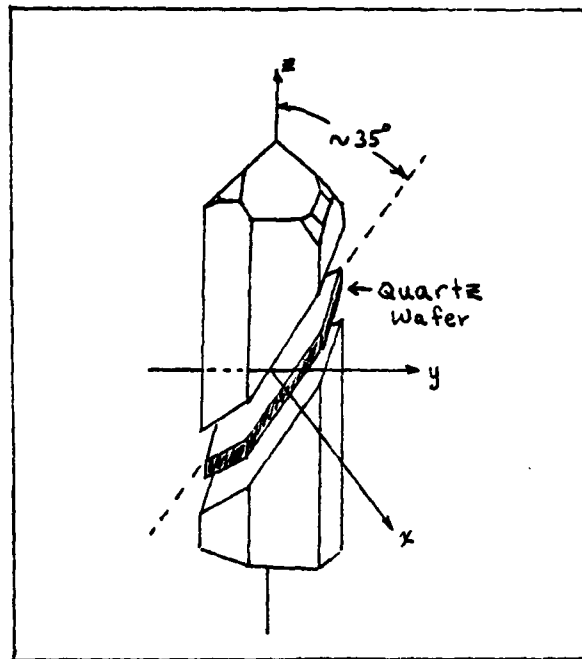


Fig. 15 AT-cut Quartz Crystal
(19;1--108)

+55°C. (3;24) The small effect on the crystal frequency by temperatures in this range can be seen in the plot in Figure 16.

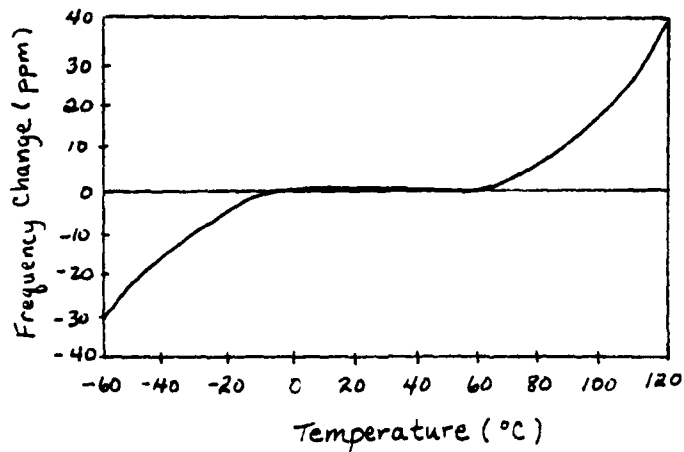


Fig. 16 Frequency Change vs
Temperature for AT-cut
Quartz Crystal (19;1--108)

When an ac field is applied to an AT-cut quartz crystal, the result is an induced thickness-shear mode of oscillation in the crystal. (16;243) The crystal wafer oscillating in this mode has a thickness which is equal to a half wavelength of the resonant frequency, usually chosen to be 5 MHz, and with its major surfaces antinodal. (3;21, 19;1--107) The resonant, or fundamental, frequency is given by

$$f = \frac{v_{tr}}{2t} \quad (51)$$

where t is the wafer thickness and v_{tr} is the velocity of the electric transverse wave in the direction of the thickness. (3;21) For AT-cut crystals $v_{tr}/2$ is a constant, N' , equal to 1670 kHz-mm (3;21) and the frequency becomes

$$f = \frac{N'}{t} \quad (52)$$

If the thickness of the quartz plate were to change, the amount of this change could be found using (3;21, 1;2)

$$dt = \frac{dm}{\rho_q A} \quad (53)$$

where ρ_q is the density of quartz ($\rho_q = 2.65 \text{ g/cm}^3$) (19;1--109), A is the area of the crystal wafer exposed to the evaporant, and dm is the amount of additional mass added to the quartz. If Eq. (52) is differentiated with respect to t and use of Eq. (53) is made, the result is (3;21, 1;2)

$$\frac{df}{dt} = - \frac{N'}{t^2}$$

$$df = - \frac{N' dm}{t^2 \rho_q A} \quad (54)$$

but

$$t = \frac{N'}{f}$$

so that

$$df = - \frac{f^2 dm}{N' \rho_q A} \quad (55)$$

Eq. (55) shows that the change in frequency experienced by the crystal is directly proportional to the amount of mass added to it. This relationship will hold for a thin film of any material deposited onto the quartz surface, provided that the mass dm is small. (3;21, 1;2) This is true because, since the quartz surfaces remain antinodes, the change in the frequency of oscillation is due only to the mass added to it, as the elastic constants of the evaporant material do not affect the crystal frequency (i.e., there is no elastic deformation energy stored by the film during oscillation). (3;21, 19;1--108, 1;2) This is the basis for using the oscillating quartz crystal as a film thickness monitor. The frequency of the crystal will change not as a result of its own thickness changing, but as a result of a change in thickness due to an equivalent mass of evaporant, dm , being added to its surface.

The quartz crystals most often used for thickness monitoring are circular or square wafers 13-14 mm wide. (19;1--111) Even though the change in pressure during pumpdown can affect the damping of the crystal oscillator, pressure variations, such as from 10^{-4} to 10^{-6} torr or those occurring during deposition of the material, will be small enough that their effect on frequency changes will be negligible if the measurements are performed in the vacuum system. (3;24, 1;3) This allows the monitor to be used in high vacuum systems.

The crystals are mounted in holders that maintain electrical contact between the crystal and its electrodes and also protect the crystals against position changes due to mechanical shocks while allowing for easy removal and replacement. (19;1--111, 1;3) Even though AT-cut crystals have a small temperature coefficient of frequency over a fairly wide range, the frequency can still be affected greatly by heat received from the evaporation source and from the heat of condensation of the evaporant. (3;24, 19;1--112) To reduce this effect, the holder for the quartz crystal is usually water-cooled. (see Figure 17)

The area of the crystal surface exposed to the vapor stream is still vulnerable to the effects of temperature even with a water-cooled holder, and Behrndt (3;25) suggests a way to minimize this effect. A mechanical shutter of some sort can be used to cover the substrate and prevent deposition onto the substrate while the material is heated to its evaporation temperature. At the same time, since it is not shuttered, the quartz crystal will feel some rise in temperature due to the

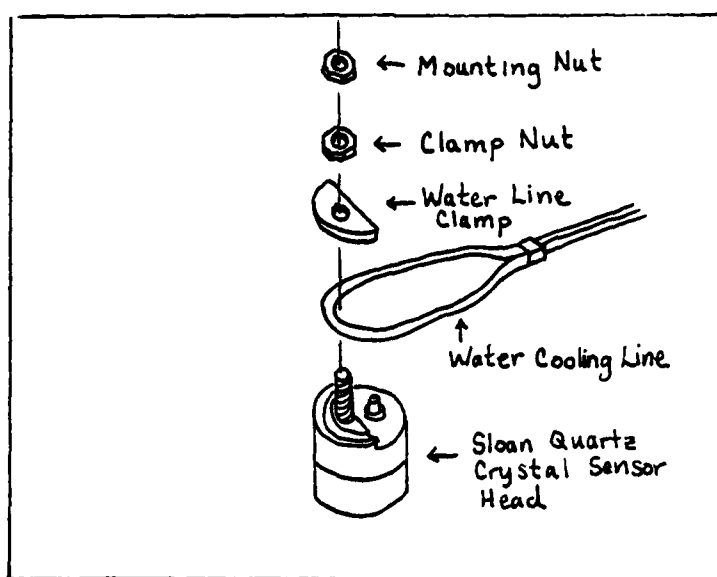


Fig. 17 Sloan Instruments Water-Cooled Quartz Crystal Sensor (22;2)

source. As the evaporation temperature is attained, opening of the shutter can be delayed for about a minute or so to allow the crystal temperature to stabilize. In this manner, the crystal has already undergone its frequency change due to temperature and is nearly at thermal equilibrium when the shutter is opened. The mass measurement will then not be affected by temperature if the change in frequency is recorded between the opening and closing of the shutter.

All that is necessary to employ a quartz crystal monitor in a thin film coating plant is an oscillator circuit to drive the crystal and a frequency meter to indicate output. (3;25, 19;1--112) More commonly, the frequency of the monitor crystal is mixed with the frequency of a constant reference oscillator to provide a difference frequency which changes as the monitor frequency changes. (3;25, 19;1--112)

For determination of deposition rate, two approaches are used depending on the type of monitor system employed. (19;1--112-13) For a digital system, the frequency output can be displayed on a printer and rate obtained by manually or automatically comparing the difference between adjacent readings, as the measurements would be taken at fixed time intervals. If analog equipment is used, the meter needle deflection is converted to a dc signal that is displayed on a strip chart recorder, where the rate is obtained by observing the slope of the plot.

Automatic control of the deposition can be achieved by allowing the monitor system to activate a relay which will shutter the substrate and turn off power to the source when the desired thickness is obtained. (19;1--113) The monitor system can also be a part of a feedback loop so that a constant deposition rate can be maintained, if desired. (3;26)

It should be remembered that the thickness determined by a quartz crystal monitor is the film's physical thickness. To obtain optical thickness, a more desired quantity, the physical thickness must be multiplied by the deposit's index of refraction. Thus, a precise knowledge of this value and the value for the material's density, which must be used to obtain physical thickness from the mass measured by the monitor, must be obtained. This is not always easy, since the density and index of the film may depart from the values given for the bulk material, as indicated in the previous chapter.

B. Sensitivity and Accuracy

The "sensitivity for mass determinations" (3;22, 1;2) of the quartz crystal oscillator is obtained from Eq. (55) as:

$$C_{f_0} = \frac{f^2}{N' \rho_q} = \frac{N'}{t^2 \rho_q} \approx \frac{f_0^2}{N' \rho_q} \quad \left(\frac{\text{Hz-cm}^2}{\text{g}} \right) \quad (56)$$

where f_0 represents the frequency of the crystal at the beginning of deposition. Since N' and ρ_q are constant, C_{f_0} varies only as the square of the starting frequency. A few values of C_{f_0} for various frequencies f_0 are given in Table I. (3;22)

Table I
Sensitivity for some Specific Starting Frequencies

f_0 (Hz)	C_{f_0} (Hz-cm ² /g)	$\frac{dm}{A}$ (g/cm ²)
1×10^6	2.26×10^6	4.42×10^{-7}
2.5×10^6	1.41×10^7	7.09×10^{-8}
5×10^6	5.63×10^7	1.77×10^{-8}
1×10^7	2.26×10^8	4.42×10^{-9}

Column 3 of Table I shows, from the use of Eq. (55), how much mass would need to be added to the crystal's surface to obtain a frequency change of 1 Hz. This is also an indication of the sensitivity of the crystal, and it can be seen that the sensitivity is high enough to measure the weight of mono-atomic layers of metals (for example, for close-packed atoms, a monolayer of Fe weighs 1.5×10^{-7} g/cm²)(1;2)

Equation (56) suggests, then, considering only sensitivity, that high-frequency crystals with thickness as small as is permitted by their fragility should be used for maximum performance, obtained as a larger frequency change per mass per unit area of evaporant deposited. (19;1--109) This, as will be seen later, is not always the case.

The accuracy of the quartz crystal monitor in thickness determinations depends on the stability of the oscillator circuit which in turn affects how sensitive the oscillator will be to changes in mass. Usually, the stability is around 10 to 100 Hz/hr, leading to a sensitivity limit of 10^{-7} to 10^{-6} g/cm² which will result in an accuracy for thickness and rate control of approximately $\pm 2\%$. (19;1--113)

C. Long Term Operation and Linearity

The relationship between mass deposited and resulting frequency change in Eq.(55) is only linear if the factor C_{f_0} , described by Eq. (56), is a constant. This will occur for changes in frequency df that are small compared to the starting frequency f_0 so that $f \approx f_0$ and the approximation made in Eq. (56) is valid. However, the basic operating principle of the quartz crystal monitor relies on a changing frequency f to detect mass deposited on its surface. Any assumption that C_{f_0} is a constant will therefore contain some error, as f must change with change in mass. The crystal frequency f is related to the starting frequency f_0 by $f = f_0 - df$ (3;23, 2; 623) where df is the measured change in frequency during the deposition. Using this relationship, then, approximately

$$\begin{aligned}
 f^2 &= f_0^2 - 2f_0 df \\
 &= f_0 (f_0 - 2df)
 \end{aligned}
 \tag{57}$$

where the df^2 term has been neglected. Substitution of Eq. (57) into (55) gives

$$\begin{aligned}
 df &= - \frac{f_0}{N' e_q A} (f_0 - 2df) dm \\
 &= - C f_0 (f_0 - 2df) dm
 \end{aligned}
 \tag{58}$$

where C now is a constant dependent on the crystal itself and equal to $1/N' e_q A$. (2;623)

Equation (58) now indicates that there is no longer a linear relationship between the mass deposited on the crystal and the resulting change in frequency. As can be seen, for cases of large layer thicknesses or continued long term use of the same oscillator crystal, there will be an increasing deviation of the relationship between dm and df from the linear relationship in Eq.(55) as df becomes larger with increased loading of the crystal. (3;23, 2;623)

If a deviation from linearity of 1% is set as a limit to where the region that approximates linear response ends, then the maximum permissible df that can occur before linearity can no longer be assumed without errors becoming significant is about 0.5% of the starting frequency. (3;23) Column 2 of Table II gives the permitted frequency shifts df that would produce a 1% deviation from linearity for the same starting frequencies used in Table I. (3;22)

Table II
Permitted Frequency Shifts for Some Specified
Starting Frequencies

f_0 (Hz)	$(df)_p$ (=0.5% f_0) (Hz)	$\left(\frac{dm}{A}\right)_p = \frac{dfN^2 \rho_q}{.99f_0^2}$ (g/cm ³)
1×10^6	5×10^3	2.23×10^{-3}
2.5×10^6	1.25×10^4	8.83×10^{-4}
5×10^6	2.5×10^4	4.41×10^{-4}
1×10^7	5×10^4	2.23×10^{-4}

As shown in the table, the maximum frequency shift allowable increases for increasing starting frequency. However, since higher frequencies increase the sensitivity as was seen from Eq. (56), smaller masses deposited will be responsible for these larger frequency shifts. This can be seen in column 3 of the table, which shows the masses corresponding to the frequency shifts indicated in column 2.

The above observation and the apparent conclusion favoring high frequency (or thin) crystals in the interest of greater sensitivity drawn from Eq. (56) lead to a necessary compromise between the amount of sensitivity required and the maximum amount of mass that can be deposited before the response is no longer linear. Crystals that are high frequency or very thin (or both) will have a higher sensitivity and a greater permissible df , but will only be able to measure small mass loads before the response becomes non-linear. Thicker, or lower frequency, crystals will be able to handle

a higher mass loading and be able to be used for longer periods of time since the mass deposited will cause smaller frequency shifts. These smaller shifts mean that it will take longer to reach its reduced permissible df (compared to higher frequency crystals), but only because it is much less sensitive. Therefore, if thinner films are to be deposited, a high sensitivity and a high frequency are desirable; if thicker films will be made, or if the crystal must be used for a long period of time, then its response should deviate from linearity as late as possible, requiring thicker crystals of low frequency. (1;2) The crystal type most often chosen as a compromise between the two extremes is a 5 to 6 MHz crystal of about .3 mm thickness. (19;1--110)

The maximum permissible df does not indicate a point at which use of the quartz crystal monitor must be stopped, it only serves as a caution that increasing errors may be experienced if linearity is assumed beyond this range. Once the maximum df has been attained, the deposits can be etched off the surface and the crystal reused, but it may be more economical and simpler to use a fresh crystal. (3;23)

A further caution about venturing beyond the maximum permissible df can be made concerning the operation of the crystal itself. As the thickness of the deposit becomes no longer small compared to the thickness of the crystal, accompanied by a larger df , the elastic components of the material deposited become important, and elastic energy can be stored by the deposit affecting the vibration characteristics of the crystal. (3;23, 19;1--111) Vibration in modes other

than the thickness-shear mode can occur and even become preferable to the fundamental mode. When this occurs, there may be significant "jumps" in the frequency of the crystal, or it may stop oscillating entirely. (3;23, 19;1--111) These conditions, however, do not limit the use of the quartz crystal as a thickness monitor, for they usually occur after several thousand angstroms or even several micrometers of material have been deposited. (3;23)

D. Optimum Usage of Quartz Crystal Oscillators

In consideration of the theory, characteristics, and limitations of the operation and use of quartz crystal oscillators for thin film thickness monitoring, Riegert presents some practices and procedures that should be followed to enhance the performance of the quartz crystal monitoring system. (21;527-30) The areas that can cause the most problems with the operation of quartz crystals are thermal, mechanical, and electrical.

Since the temperature coefficient of frequency is near zero in only a small temperature range for a particular cut of the crystal, it is necessary to guard against temperature drifts which may affect the frequency of the crystal's oscillation. Riegert suggests that the crystal should be operated at a temperature below 120°C for maximum reliability. (21;527) Otherwise, thermal effects will cause expansion of the Si and O bonds in the quartz, leading to possible oscillation in unwanted modes or directions, or even induced jumps in the crystal's frequency. Thermal effects on the crystal

can be reduced by mounting the crystal on a copper block that will serve as a heat sink and store energy away from the crystal, water cooling the crystal holder, or optically shielding the crystal from some of the energy emitted by the source. (21;528) Also, the procedure described by Behrndt in section A, using a mechanical shutter over the substrate to allow the the crystal to come to thermal equilibrium before use, can be employed.

Mechanical effects, such as the effect on linearity of the crystal's response under long term use or loading has been discussed in the previous section. A heavily loaded crystal may eventually fail to operate. The obvious solution here is to replace it with a fresh crystal to insure reliable measurements.

Harmful electrical effects on the crystal oscillator may result if high enough amounts of stray charge build up on the crystal surface from sources such as a faulty electron gun, glow discharges, sputtering sources, and rf induction equipment. Component failure in the crystal oscillator or the reference oscillator may result if steps are not taken to collect stray charges or shield the crystal from them. (21;529) Finally, to isolate the rf signal of the crystal oscillator and protect against high frequency loss in the electrical signal, cabling internal to the vacuum system should be no more than 3 ft in length, or less, if possible. The external cable should be coaxial to prevent unshielded single wires acting as antennae for external rf, such as local fm radio stations. (21; 529-30)

VI Experimental Arrangement

Based on the theory of operation discussed for both the optical monitor and the quartz crystal monitor, equipment and apparatus were obtained for the employment of both of these monitoring methods in the thin film evaporation plant described in Chapter III. This chapter will describe the arrangement and use of the components of both of these systems.

A block diagram showing the path and major components of the optical monitoring system is presented in Figure 18.

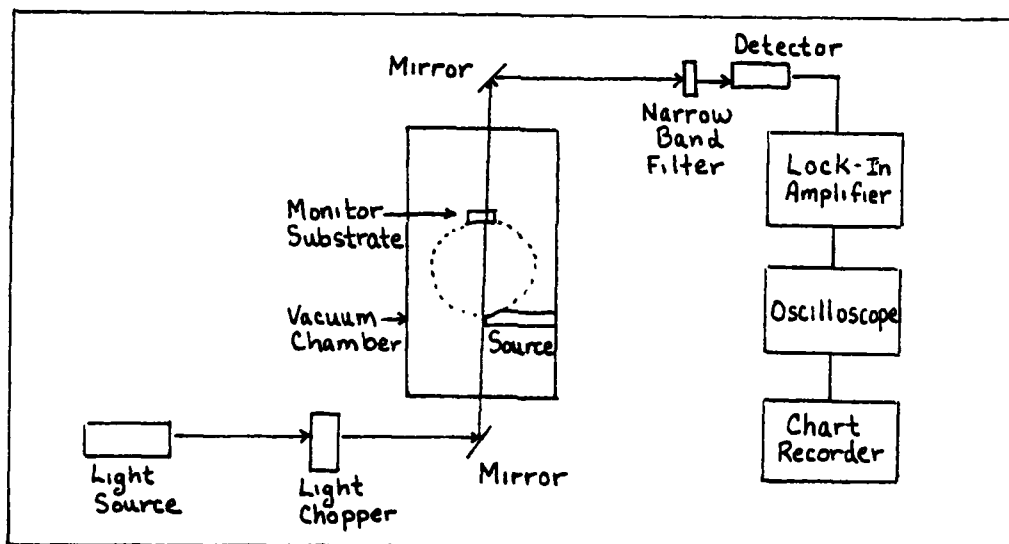


Fig. 18 Optical Monitoring System

The light source should, for maximum flexibility, be white light. Then, in order to choose a specific monitor wavelength determined by the purpose of the film to be produced, all that is necessary is the correct narrow-band filter in front of the detector. A laser may be used for a monochromatic source, but this limits the monitor wavelength to that of the laser.

Any other wavelength desired requires the use of a different laser.

If a white light source is used, it must also be collimated to enable most of the light's intensity to pass through the system. In this system, a General Electric tungsten filament projector bulb (6V, 3.5 A giving about 21 watts) was used as the source. To collimate the light, a 150 mm focal length lens was placed 55.5 cm from the source, producing an image of the filament 20.5 cm from the lens. At this focal point, a variable aperture adjusted to its smallest size of 1.2 mm diameter was placed to serve as a point source of white light. Fifteen centimeters from the point source, another 150 mm focal length lens was placed to provide a collimated white light beam of about 3 cm diameter.

For the use of a laser light source, a Melles Griot model 05 LLP 805 .5 mW ($\pm 2\%$) He-Ne laser provided light at 632.8 nm in a beam of .59 mm diameter with divergence ($1/e^2$) of 1.3 mrad. (20) Collimation was not used for this source.

The source light beam then passed through an EG&G Princeton Applied Research model 192 Variable Frequency Light Chopper set at 80 Hz. The light is chopped at a known frequency before it enters the system so that it can be discriminated from other sources of light such as ion gauge or electron gun filaments that may affect the measured signal.

After chopping, the light is directed by a neutral density filter of OD 3 ($T = 1/1000$) acting as a fold mirror so that it will ideally pass vertically through the chamber along its axis, where the monitor substrate is located. The light

will then be incident on the substrate normally, which is the condition described in Chapter IV on optical monitoring. The geometry of the vacuum chamber did not allow this ideal condition exactly, but what was obtained was close to that desired. The beam's path through the chamber is shown in Figure 19.

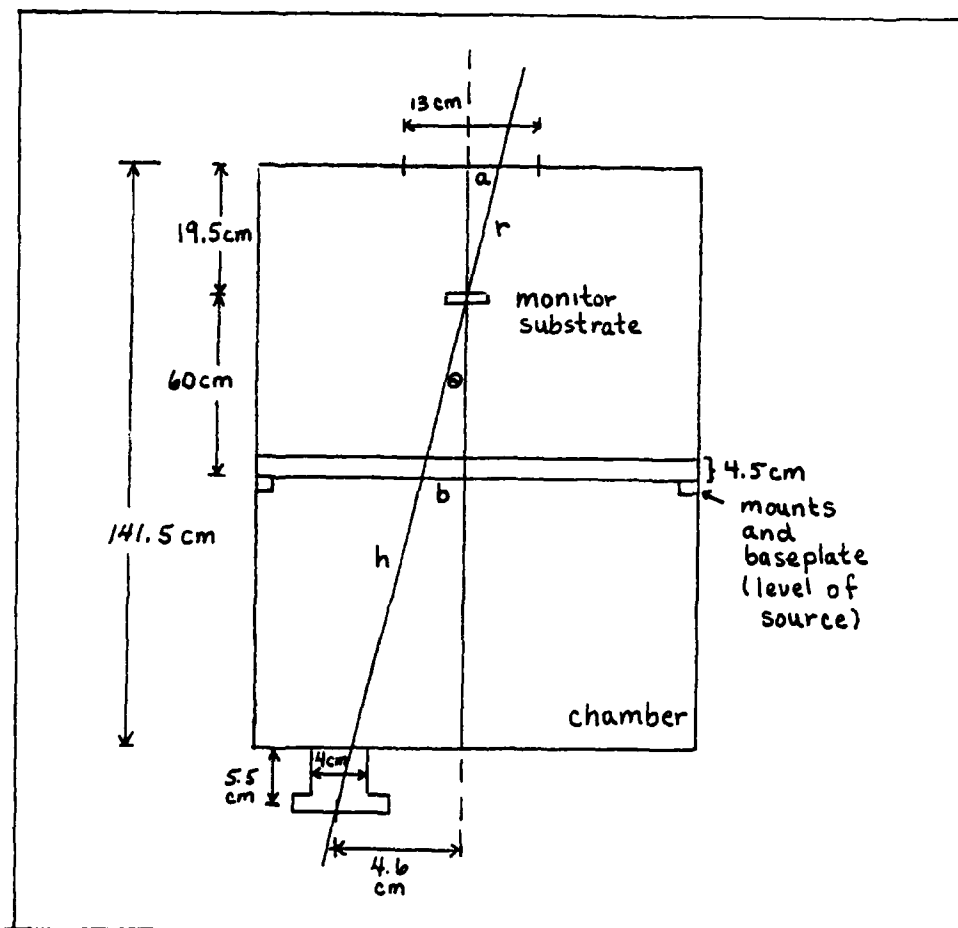


Fig. 19 Optical Path Through System

The angle that the actual path deviates from the desired path (the center line, or axis) is determined to be 1.98° . The monitor wavelength will be shifted to a slightly longer

wavelength dependent on the cosine of the angle of incidence:

$$\begin{aligned}\lambda' &= \frac{\lambda}{\cos \theta} = \frac{\lambda}{.9994} \\ &= (1.0006)\lambda\end{aligned}\tag{59}$$

where λ' is the effective monitoring wavelength.

After exiting the top viewing port of the vacuum chamber, the light beam is directed by a mirror to the narrow band filter/detector combination located on a table top surface mounted to the top of the equipment rack of the VI-360 vacuum system. Two narrow band filters were available for use with the white light source. These were located at 628.4 nm and 530.0 nm, both having linewidths of about 10.0 nm and transmission at their peak wavelengths of 23% and 20.7% respectively, determined using the profiles obtained with a Perkin Elmer model 350 Spectrophotometer. The detector was an EG&G Electro-optics FND-100 silicon photodiode. It is useful in the 300 - 1100 nm wavelength range, with a responsivity of .62 A/w at 900 nm, its peak. (6)

The modulated ac signal received by the detector is then sent to a Keithley Instruments model 840 AutolocTM Amplifier. Here, the 80 Hz signal is separated from that of other, unwanted sources, demodulated, and amplified to a ± 10 Vdc output which is displayed on a Ballantine 1066S Oscilloscope. The change in signal magnitude is tracked and recorded on an E.H. Sargent & Co. model SR chart recorder.

The use of the strip chart recorder to display the output transmittance or reflectance signal is recommended, (16; 238) rather than observing the motion of an analog needle, in order to obtain increased accuracy using the turning value method of thickness monitoring. The eye will tend to smooth out the curve and extrapolate ahead, making it easier to determine the turning points. Using this method, the operator, with some practice, should be able to terminate the layers within 5-10 percent of the turning point on the monitor substrate, depending on the film's index. (16;238) The actual accuracy in thickness and reflectance will then depend on the over- or undershoot in the manner described earlier.

The sensor used in the quartz crystal monitoring system is the Sloan Instruments Corp. number 103-850 Quartz Crystal Sensor Head. It is a stainless steel housing consisting of an oscillator head and a cap which holds the crystal and maintains the crystal's contact with the signal connectors on the oscillator housing. The quartz crystal is a Sloan 103-872 5-MHz crystal of 1.2 cm diameter and .35 mm thickness. The sensing unit is mounted inside the vacuum chamber, adjacent to the center substrate holder location (see Figure 5), so that the sensor head is oriented vertically and the crystal surface exposed to the vapor stream is at the same height as the substrate surface. The sensor head is connected by coaxial cable to a Sloan DTM-3 deposit thickness monitor that displays a difference frequency between the crystal oscillator frequency and that of the variable frequency reference oscillator.

As the deposition proceeds, the difference between the crystal oscillator and the reference, initially at zero, will increase. The change in frequency can be related to the thickness t deposited of material of bulk density ρ by starting with Eq. (55) of Chapter V:

$$\Delta f = - \frac{f^2 dm}{N' \rho_f A} \quad (60)$$

The mass of film deposited can be expressed as

$$dm = t A \rho_f \quad (61)$$

and upon substitution into Eq. (60), Δf becomes

$$\Delta f = - \frac{f^2 t \rho_f}{N' \rho_f} \quad (62)$$

Solving for the film thickness, this becomes

$$t = - \frac{N' \rho_f \Delta f}{\rho_f f^2} \quad (63)$$

Using the values given earlier, $N' = 1670$ kHz-mm, $\rho_f = 2.65$ g/cm³, and $f = 5 \times 10^6$ Hz, the expression is

$$\begin{aligned} t &= -1.77 \times 10^{-8} \frac{\Delta f}{\rho_f} \quad (\text{cm}) \\ &= \frac{-1.77 \Delta f}{\rho_f} \quad (\text{\AA}) \quad (64) \end{aligned}$$

VII Results

The quartz crystal monitoring system was used as described in the previous chapter, and the original optical monitor was to employ the white light source and the 628.4 nm narrow band filter. After the light source, collimation optics, chopper, detector, amplifier and recorder were installed on the system and aligned, a test was run to see how the system responded when a graded, neutral density filter was placed in the beam before the detector and rotated at a rate of .5 rpm. The neutral density filter varied from .014 (T=96.8%) to 1.5 (T=3.1%) and the response of the system is shown in the recorder trace of Figure 20. From this trace, the rapidly varying portion of the signal with the appearance of noise was determined, by comparison, to be about 10-12% of the maximum signal indicated by the trace. The reason for the magnitude of this "noise" or its origin were not known.

The narrow band filter was next inserted to observe its effect and since its transmittance is only about 23% at its peak wavelength, the resulting signal to the detector was considered too small (~.5V on the 1-10V amplifier output) to be useful in detecting accurately the turning points encountered during deposition. This led to the use of the He-Ne laser at 632.8 nm for the light source and monitoring wavelength of the optical monitoring system. The resulting recorder trace of a similar test using this light source and the variable neutral density filter is shown in Figure 21.

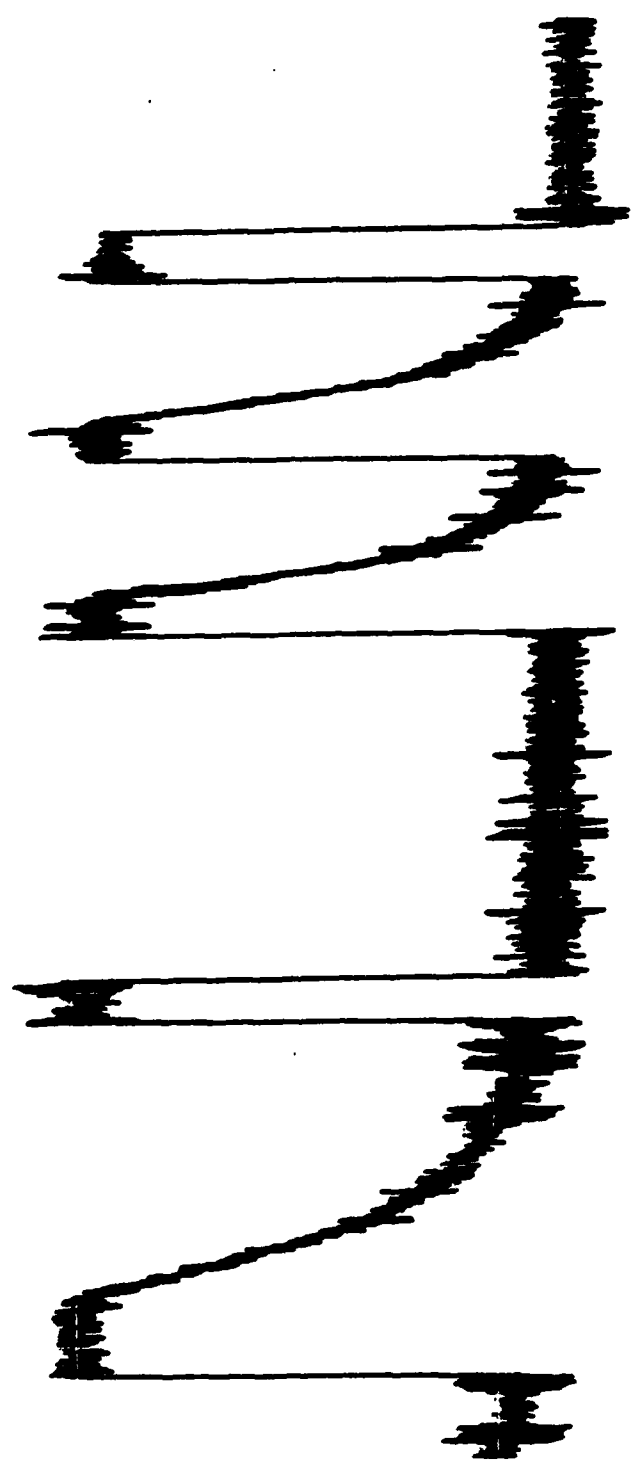


Fig. 20 Optical Monitor Response Test with White Light Source
(Signal Amplitude plotted versus Time)

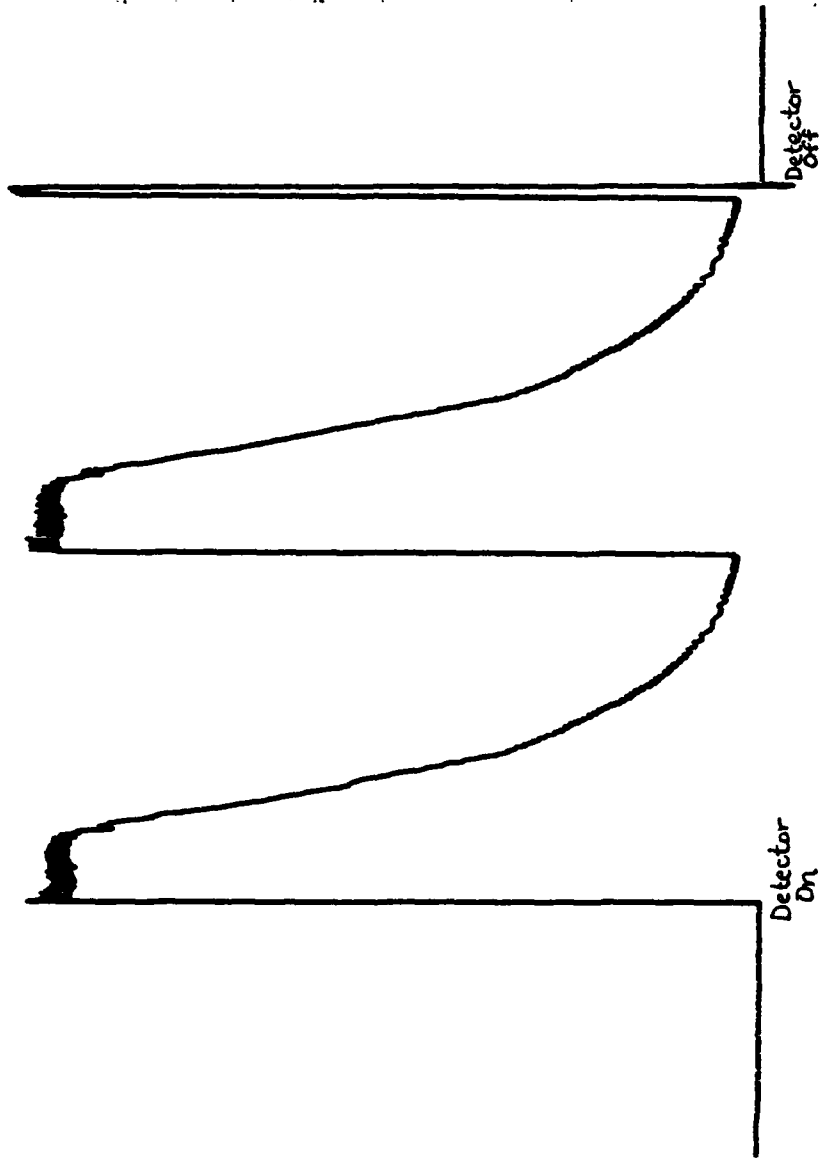


Fig. 21 Optical Monitor Response Test with He-Ne Laser
(Signal Amplitude plotted versus Time)

After the monitoring system was finalized, MgF_2 was selected to be evaporated using the electron gun source. MgF_2 has a density of 3.148 g/cm^3 and an index of refraction of 1.38. (10) The electron gun was modified with four 4.5 cm rods made from steel (non-stainless) nails to act as keeper bar shunts when placed across the crucible divider walls on the side of the gun opposite the filament to modify the magnetic field enough to cause the electron beam to fall properly in the center of the crucible. This modification was necessary due to suspected magnetic field strength change possibly due to the age of the device.

Using Eq. (64) for the relationship between thickness and frequency change in the quartz crystal monitor, the desired frequency change was determined for the deposition of a quarter wave of MgF_2 at $\lambda = 632.8 \text{ nm}$. This value was determined to be 2.04 kHz when an f_0 of 5 MHz is assumed.

The change in transmittance expected to be recorded by the optical monitoring system was calculated to run from 92% for the bare substrate to 94.6% after the first quarter wave, 92% again after a half wave, and then ideally alternate in a sinusoidal pattern between 94.6% and 92% for each additional quarter wave deposited.

MgF_2 was evaporated by the electron gun until the desired frequency change was recorded by the quartz crystal frequency meter, indicating that a quarter wave had been deposited. This was accomplished, satisfying questions as to whether the shallow crucible of the electron gun would hold enough material to deposit a quarter wave. The "noise" observed on the recorder

trace, as mentioned earlier, was now about 3% of the total amplitude on the average, which would make determination of a change in transmittance from 92% to 94.6% nearly impossible. There was a steady drift noted in the output of the recorder, and correction for this at the end of the run where the detector was turned off indicated that the signal at the point where the quartz monitor recorded a quarter wave was about 99% of its original value. It was then decided that another material of higher index than that of glass be used to obtain a greater range in transmittance between successive turning values.

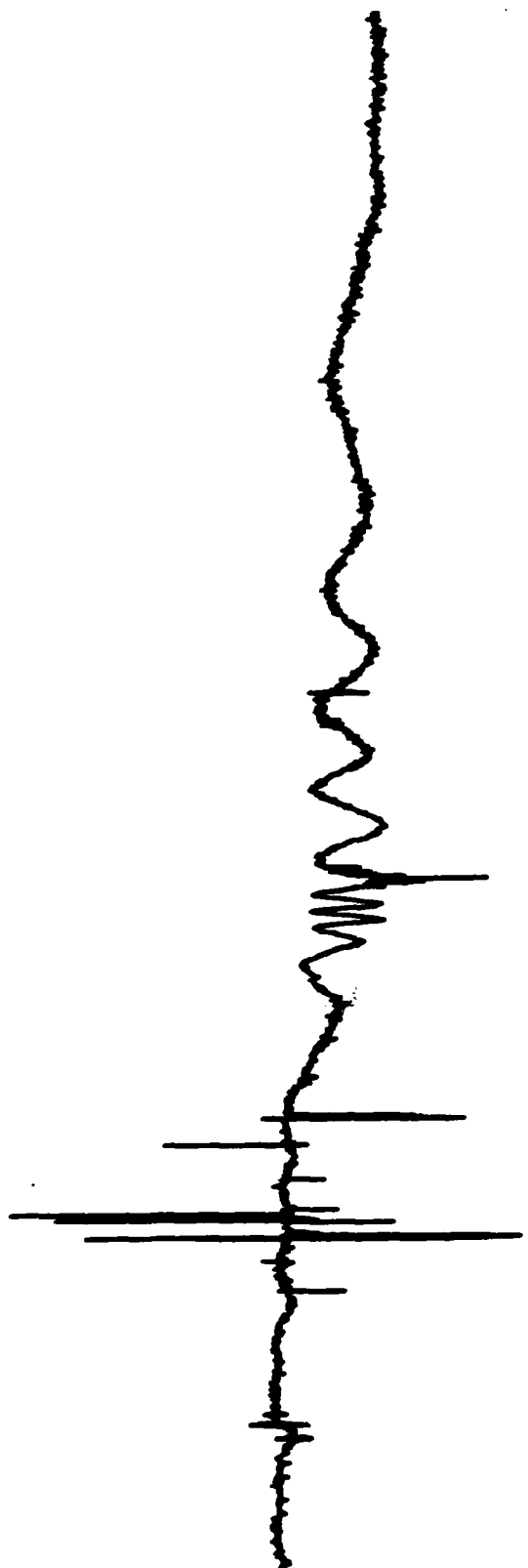
The high index material chosen to be evaporated was TiO_2 . It has an index of 2.58 and a density of 4.17 g/cm^3 . (7;B-159) Its transmittance will range from 92% for the bare substrate, to 56% after a quarter wave, to 92% for a half wave, and then alternate ideally between 56% and 92% thereafter. Eq. (64) predicts a frequency change of 1.44 kHz for the deposition of a quarter wave to be accomplished.

During the deposition of the TiO_2 , the optical signal "noise" level was estimated to be around 1%, possibly due to better alignment of the laser beam through the system (the mirror located on top of the chamber must be removed and then realigned each time the chamber is opened). As the quartz crystal monitor reached the expected frequency change indicative of the deposition of a quarter wave layer, it was evident that the optical monitor was nearing a turning value. The peak of this point was observed when the frequency meter

indicated 2100 Hz. The recorder trace produced during this deposition run is shown in Figure 22.

From the trace it was seen that there was still a drift in the recorder output which, for the analysis of the results obtained, was assumed to be constant with time. The several large spikes appearing just before the first turning value were most likely due to arcing that was observed to occur periodically between the electrodes that supply power to the electron gun. After the first turning point was reached, it appeared that several turning points were produced in rapid succession accompanied by a rapid increase in the difference frequency displayed by the crystal monitor. Unfortunately, the rapidity of these events and the physical distance between frequency meter and chart recorder were such that frequency readings for these peaks were not obtained. The several sharp turning points after the quarter wave turning point are unexplainable and believed not to be actual turning points. The spike immediately following these points is again probably due to another arc occurring. The smoother turning points following this resemble the first one and may be additional actual turning points, indicating that as many as five quarter waves may have been deposited before the high voltage was turned off.

Only the turning point for the first quarter wave layer was analyzed to determine how well the measured values approached the calculated predictions. Taking the drift of the recorder into account, it was determined that the peak of the turning point represented a signal that was 86.9% of the original



- H.V. off
- 2100 Hz
- freq relay activates - 1450 Hz
- Quartz meter audio begins
- H.V. on

Fig. 22 Optical Monitor Output for TiO_2 Deposition Run
(Signal Amplitude plotted vs time)

signal. Since the original signal was assumed to represent the 92% transmittance for the bare substrate, the transmittance of the turning point was determined to be approximately equal to 80%.

From the values obtained from the TiO_2 deposition run, it was clear that the expected quartz crystal frequency change and the optical transmittance were not the values predicted by the calculations. If Eq. (64) is used and 2100 Hz is substituted for the expected change in frequency, solving for the constant gives a value of 1.22 instead of 1.77. This may suggest a slightly different value for N' , which would be so if a crystal cut other than AT was used for these crystals, since the AT-cut was assumed here. If, in fact, 2100 Hz is the correct value, rather than 1440 Hz, and the value for N' is also correct, then solving Eq. (64) for the thickness gives a value of 89.137 nm. If this value is then used with the optical thickness for a quarter wave layer at 623.8 nm, then the index of refraction would have to be equal to 1.77. This value seems too low, even if decomposition of the TiO_2 is considered to have occurred during evaporation. It should be noted that a material of index 1.87 would result in a transmission of 80%, the value obtained experimentally.

A second deposition run with TiO_2 produced features on the optical monitor output trace that resembled turning points, but not in the manner expected. At the point where the desired frequency change in the quartz crystal was reached, no obvious turning points were noted. In fact, no recorder motions even resembling turning points were noticed until much

later. While the response of the system at these points is of the shape expected for turning points, the number that were produced made it hard to believe that several quarter wave layers could have been deposited. Evidence to the contrary, though, was that there was still unevaporated material left in the crucible at the end of the deposition run. The delay in the appearance of these apparent turning points could be due to a lag in the response of the detector, but this seems unlikely and would not support the results of the first run, which were much closer to the response expected. From this second run, it can only be said that the optical system appears to be responding as it should during the deposition of successive quarter wave layers, but the great difference in the results of the two deposition attempts are unexplainable.

VIII Conclusion and Recommendations

This investigation was designed to produce a thin film coating plant that employed thickness monitoring techniques for control of the deposition process. The basic objective has been accomplished. The vacuum system was fitted with the equipment necessary to mount substrates, evaporate sources, and monitor the thickness of the deposit during the process. Thickness monitoring using the optical technique of turning value monitoring and using a quartz crystal oscillator was performed to demonstrate the response of both systems as a film was deposited on a substrate; however, the monitoring systems were not calibrated and their separate outputs were not able to be correlated to each other. Ideally, the two systems, working independently, should have indicated the deposition of a quarter wave layer at the same time. This condition was not achieved and the apparent indication of a quarter wave layer by the two systems, while both responded in the manner expected, did not occur at the point predicted by theory. As the optical system measured optical thickness, and the quartz crystal measured physical thickness, related to each other by the film's index of refraction which was most likely different than the bulk properties assumed, there was no way to correlate the results without further testing or to pinpoint which of the systems was in error.

The results obtained indicate that the basic design of the system and the operation of the various equipment involved is such that the monitoring systems were able to apparently

respond properly, but not to the extent that reliable coatings could be made. As time was limited to demonstrate a workable system, and from the experience of assembling the plant's various components, a number of recommendations can be made for improvement or continued use of the present system.

Concerning the white light version of the optical monitor, its effective use requires a more intense light source as a starting point. 600 W Quartzene lamps were located late in the project that may be useful, however, a housing to hold the bulb and provide electrodes for its power along with a fan for cooling would need to be designed and built. A complete set of narrow band filters must also be obtained to give the system the desired flexibility of choice in monitoring wavelength. An improved chart recorder with no drift may also prove necessary. If these components cannot be provided separately, it may be required to purchase a commercial optical monitor package.

The sensor heads for the quartz crystal monitoring system owned by the department should either be repaired or replaced, as the one used in the final system was loaned by a source outside of AFIT. Should this not be possible, a new quartz crystal system would need to be obtained. The system eventually put into use should be calibrated for the various materials that may in the future be used to produce coatings.

The evaporation source, the electron gun, should have its magnet restored, replaced with one of the proper strength, or a new gun obtained. Documentation concerning the replacement

of filaments and the focusing of the beam should be included in particular. A variety of coating grade, or high purity, materials should be purchased in order to be able to make coatings for various requirements.

Further test depositions should be conducted using both monitoring systems so that correlations can be made between the output produced by these systems in order to provide more reliable and dependable results. Separate deposition runs should be made with monitoring using only one system at a time and then the results tested using a physical thickness measurement process or some other post-deposition thickness measurement. The results may show which of the systems is producing more reliable results, or indicate sources of error.

Obtaining and maintaining in proper working condition the equipment mentioned in these recommendations will help improve the utility and versatility of a thin film coating plant that can become an important apparatus in future research and instructional projects.

Appendix

Derivation of the Characteristic Matrix for a Thin Film

The following derivation is an adaptation of the one presented by Macleod (16;17-18)

For normal incidence onto a thin film on the surface of a substrate, the situation is as illustrated in Figure 23.

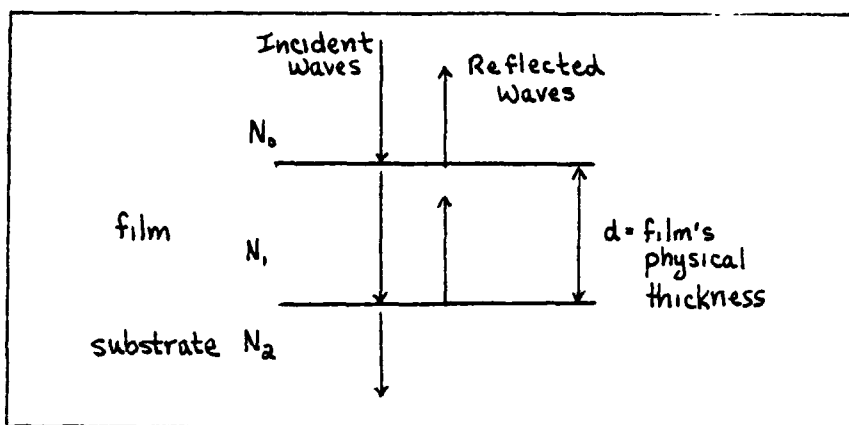


Fig. 23 Interaction of Radiation with
Film-Substrate Combination

In the following, waves in the direction of the incident wave will be termed positive-going, and waves in the opposite direction will be termed negative-going. (16;12) There are two waves in the incident medium: one positive-going incident wave and one negative-going reflected wave. In the film there is a positive-going transmitted wave and a negative-going wave reflected from the boundary with the substrate. The substrate only contains a positive-going transmitted wave. Each of the waves consist of a magnetic component \vec{H} and an electric component \vec{E} , with the boundary condition that the tangential

components of \vec{E} and \vec{H} across any boundary be continuous.

At the film-substrate boundary,

$$\left. \begin{aligned} \vec{H}_1 &= \vec{H}_{2t}^+ = \vec{H}_{1i}^+ + \vec{H}_{1r}^- = N_1(\vec{k} \times \vec{E}_1^+) + N_1(-\vec{k} \times \vec{E}_1^-) \\ \vec{E}_1 &= \vec{E}_{2t}^+ = \vec{E}_{1i}^+ + \vec{E}_{1r}^- \end{aligned} \right\} (65)$$

where the subscripts t, i, and r represent transmitted, incident, and reflected waves, respectively.

If

$$\vec{k} \times \vec{E}_1 = (\vec{k} \times \vec{E}_{1i}^+) + (\vec{k} \times \vec{E}_{1r}^-)$$

then, using Eq. (65),

$$\begin{aligned} \frac{\vec{H}_1}{N_1} &= \vec{k} \times \vec{E}_{1i}^+ - \vec{k} \times \vec{E}_{1r}^- \\ &= \vec{k} \times \vec{E}_1 - \vec{k} \times \vec{E}_{1r}^- - \vec{k} \times \vec{E}_{1r}^- \\ &= \vec{k} \times \vec{E}_1 - 2(\vec{k} \times \vec{E}_{1r}^-) \end{aligned}$$

Thus,

$$2(\vec{k} \times \vec{E}_{1r}^-) = -\frac{\vec{H}_1}{N_1} + \vec{k} \times \vec{E}_1 \quad (66)$$

Similarly,

$$2(\vec{k} \times \vec{E}_{1i}^+) = \frac{\vec{H}_1}{N_1} + \vec{k} \times \vec{E}_1 \quad (67)$$

The waves \vec{E}_1 and \vec{H}_1 are illustrated traversing the film thickness in Figure 24.

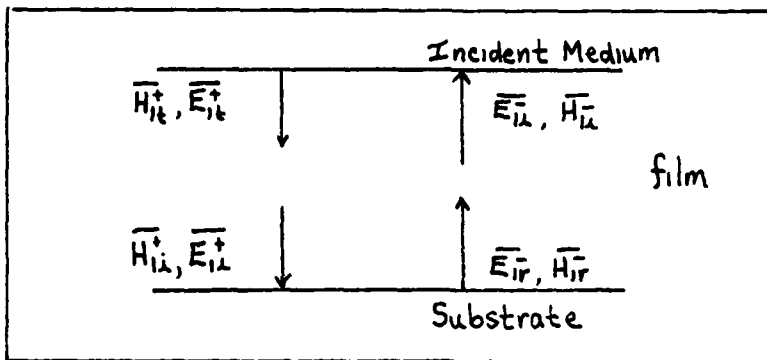


Fig. 24 \bar{H} and \bar{E} waves within the Film Thickness

In traversing the film's thickness, the waves suffer a phase shift of

$$\delta = \frac{2\pi}{\lambda} N_1 d$$

such that

$$\left. \begin{aligned} \bar{E}_{i2}^+ &= \bar{E}_{it}^+ e^{-i\delta} \\ \bar{H}_{i2}^+ &= \bar{H}_{it}^+ e^{-i\delta} \end{aligned} \right\} (68)$$

and

$$\left. \begin{aligned} \bar{E}_{i2}^- &= \bar{E}_{ir}^- e^{-i\delta} \\ \bar{H}_{i2}^- &= \bar{H}_{ir}^- e^{-i\delta} \end{aligned} \right\} (69)$$

At the incident medium-film interface, then,

$$\begin{aligned} \bar{E}_o &= \bar{E}_{it}^+ + \bar{E}_{i2}^- \\ &= \bar{E}_{it}^+ e^{i\delta} + \bar{E}_{ir}^- e^{-i\delta} \end{aligned} \quad (70)$$

$$\begin{aligned}
\bar{k} \times \bar{E}_0 &= (\bar{k} \times \bar{E}_{i\lambda}^+) e^{i\delta} + (\bar{k} \times \bar{E}_{ir}^-) e^{-i\delta} \\
&= \frac{1}{2} \left(\frac{\bar{H}_1}{N_1} + \bar{k} \times \bar{E}_1 \right) e^{i\delta} + \frac{1}{2} \left(-\frac{\bar{H}_1}{N_1} + \bar{k} \times \bar{E}_1 \right) e^{-i\delta} \quad \left[\begin{array}{l} \text{from (66)} \\ \text{and (67)} \end{array} \right] \\
&= \frac{\bar{H}_1}{N_1} \left(\frac{e^{i\delta} - e^{-i\delta}}{2} \right) + \bar{k} \times \bar{E}_1 \left(\frac{e^{i\delta} + e^{-i\delta}}{2} \right) \\
&= \frac{\bar{H}_1}{N_1} i \sin \delta + (\bar{k} \times \bar{E}_1) \cos \delta \quad (71)
\end{aligned}$$

Also,

$$\begin{aligned}
\bar{H}_0 &= \bar{H}_{i\lambda}^+ + \bar{H}_{ir}^- \quad (72) \\
&= \bar{H}_{i\lambda}^+ e^{i\delta} + \bar{H}_{ir}^- e^{-i\delta} \\
&= N_1 (\bar{k} \times \bar{E}_{i\lambda}^+) e^{i\delta} + N_1 (-\bar{k} \times \bar{E}_{ir}^-) e^{-i\delta} \quad \left[\text{from (65)} \right] \\
&= \frac{N_1}{2} \left(\frac{\bar{H}_1}{N_1} + \bar{k} \times \bar{E}_1 \right) e^{i\delta} - \frac{N_1}{2} \left(-\frac{\bar{H}_1}{N_1} + \bar{k} \times \bar{E}_1 \right) e^{-i\delta} \\
&= \bar{H}_1 \left(\frac{e^{i\delta} + e^{-i\delta}}{2} \right) + N_1 (\bar{k} \times \bar{E}_1) \left(\frac{e^{i\delta} - e^{-i\delta}}{2} \right) \\
&= \bar{H}_1 \cos \delta + N_1 (\bar{k} \times \bar{E}_1) i \sin \delta \quad (73)
\end{aligned}$$

Writing this in matrix form gives:

$$\begin{bmatrix} \bar{k} \times \bar{E}_0 \\ \bar{H}_0 \end{bmatrix} = \begin{bmatrix} \cos \delta & \frac{i \sin \delta}{N_1} \\ N_1 i \sin \delta & \cos \delta \end{bmatrix} \begin{bmatrix} \bar{k} \times \bar{E}_1 \\ \bar{H}_1 \end{bmatrix} \quad (74)$$

Since the boundary condition states that the tangential components of \bar{E} and \bar{H} are continuous across the boundaries,

E_2 and H_2 can be substituted for E_1 and H_1 to relate the waves at the interface with the incident medium to the waves transmitted through the film-substrate interface into the substrate.

The matrix

$$\begin{bmatrix} \cos \delta & \frac{i \sin \delta}{N_1} \\ N_1 i \sin \delta & \cos \delta \end{bmatrix}$$

is known as the characteristic matrix of the thin film.

Bibliography

1. Behrndt, K.H. and R.W. Love. "Automatic Control of Film-deposition Rate with the Crystal Oscillator for Preparation of Alloy Films," Vacuum, 12:1-9 (1962).
2. Behrndt, K.H. "Long Term Operation of Crystal Oscillators in Thin-Film Deposition," The Journal of Vacuum Science and Technology, 8:622-626, (1971).
3. Behrndt, K.H. Physics of Thin Films, Vol 3, ed. G. Hass and R.E. Thun, New York, Academic Press, 1966, p. 1-59.
4. Berry, R.W., P.M. Hall and M.T. Harris. Thin Film Technology, Van Nostrand Reinhold Company, New York, 1968.
5. Bousquet, P. and E. Pelletier. "Optical Thin Film Monitoring - Recent Advances and Limitations" Thin Solid Films, 77: 165-179, (1981).
6. EG&G Electro-optics Data Sheet D301 3B-1, FND-100.
7. Handbook of Chemistry and Physics, 63rd ed., CRC Press, Inc., 1982-83.
8. Holland, L. Vacuum Deposition of Thin Films, John Wiley & Sons, Inc., New York, 1958.
9. Knudsen, M. The Kinetic Theory of Gases, Methuen & Co., Ltd., London, 1934.
10. Lange's Handbook of Chemistry, 12th ed., ed. J.A. Dean, Mc-Graw-Hill, 1979.
11. Macleod, H.A. "Absorption in Turning Value Monitoring of Narrow Band Thin-Film Optical Filters," Optica Acta, 20: 493-508, (1973).
12. Macleod, H.A. "Monitoring of Optical Coatings," Applied Optics, 20: 82-89, (1981).
13. Macleod, H.A. and D. Richmond. "The effect of errors in the Optical Monitoring of Narrow-Band All-Dielectric Thin Film Optical Filters," Optica Acta, 21: 429-443, (1974).
14. Macleod, H.A. "The Monitoring of Thin Films for Optical Purposes," Vacuum, 27: 383-390, (1977).
15. Macleod, H.A. "Thin Film Narrow Band Optical Filters," Thin Solid Films, 34: 335-342, (1976).

16. Macleod, H.A. Thin Film Optical Filters, American Elsevier Pub. Co., Inc., 1969.
17. Macleod, H.A. "Thin Film Optics", Course Notes, Optical Sciences Center, University of Arizona, (1982).
18. Macleod, H.A. "Turning Value Monitoring of Narrow-Band All-Dielectric Thin-Film Optical Filters," Optica Acta, 19: 1-28, (1972).
19. Maissel, L.I. and R. Glang. Handbook of Thin Film Technology, McGraw-Hill, 1970, 1--107 - 1--113.
20. Melles Griot Operating Instructions for the .5mW Self Contained HeNe Lasers Model 05-LLR-805 and 05-LLP-805.
21. Riegert, R.P. "Optimum Usage of Quartz-Crystal Monitor-Based Devices," Proc. of the Fourth International Vacuum Congress, 527-530, (1968).
22. Sloan Instruments Corp. Installation Instructions for the Quartz Crystal Sensor Head, Part No. 103-850.
23. Standard Mathematical Tables, 24th ed., CRC Press, Cleveland, 1976.
24. Varian Associates Instruction Manual 87-400 158, VacSorb Pumps, (Nov 1966).
25. Varian Associates Instruction Manual 87-400 130, New Large Cell VacIon Pumps, (Dec 1965).
26. Varian Associates Instruction Manual for the Hastings Vacuum Gauge, 87-400 149.
27. Varian Associates Instruction Manual 87-400 174, Helmer Gauge and Helmer Gauge Control Unit, (Jul 1967).
28. Varian Associates Product Description, 2kW e-Gun Evaporation Source.

VITA

First Lieutenant John J. Eric was born on 26 June 1959 in Johnson City, New York. He graduated from high school in Johnson City in 1977 and attended the Air Force Academy from which he received the degree of Bachelor of Science in Physics in May, 1981. Upon graduation, he was commissioned as a second lieutenant in the USAF. He was assigned to the Rome Air Development Center, Griffiss AFB, NY from July, 1981 to May, 1983, when he entered the School of Engineering, Air Force Institute of Technology.

Permanent Address: 5 Plymouth St.
Johnson City,
New York 13790

UNCLASSIFIED

SECURITY CLASSIFICATION OF THIS PAGE

REPORT DOCUMENTATION PAGE

1a. REPORT SECURITY CLASSIFICATION UNCLASSIFIED		1b. RESTRICTIVE MARKINGS	
2a. SECURITY CLASSIFICATION AUTHORITY		3. DISTRIBUTION/AVAILABILITY OF REPORT Approved for public release; distribution unlimited	
2b. DECLASSIFICATION/DOWNGRADING SCHEDULE			
4. PERFORMING ORGANIZATION REPORT NUMBER(S) AFIT/GEP/PH/84-D-3		5. MONITORING ORGANIZATION REPORT NUMBER(S)	
6a. NAME OF PERFORMING ORGANIZATION School of Engineering AF Inst. of Technology	6b. OFFICE SYMBOL (If applicable) AFIT/EN	7a. NAME OF MONITORING ORGANIZATION	
6c. ADDRESS (City, State and ZIP Code) Wright-Patterson AFB, OH 45433		7b. ADDRESS (City, State and ZIP Code)	
8a. NAME OF FUNDING/SPONSORING ORGANIZATION	8b. OFFICE SYMBOL (If applicable)	9. PROCUREMENT INSTRUMENT IDENTIFICATION NUMBER	
8c. ADDRESS (City, State and ZIP Code)		10. SOURCE OF FUNDING NOS.	
		PROGRAM ELEMENT NO.	PROJECT NO.
		TASK NO.	WORK UNIT NO.
11. TITLE (Include Security Classification) See Box 19			
12. PERSONAL AUTHOR(S) John J. Eric, B.S., 1st Lt, USAF			
13a. TYPE OF REPORT MS Thesis	13b. TIME COVERED FROM _____ TO _____	14. DATE OF REPORT (Yr., Mo., Day) 1984 December	15. PAGE COUNT 93
16. SUPPLEMENTARY NOTATION			
17. COSATI CODES		18. SUBJECT TERMS (Continue on reverse if necessary and identify by block number)	
FIELD 20	GROUP 06	SUB. GR. Thin Films, Optical Coatings, Thickness, Monitoring, Vacuum Chambers	
19. ABSTRACT (Continue on reverse if necessary and identify by block number)			
Title: A THIN FILM COATING PLANT USING THICKNESS MONITORING		Thesis Chairman: John J. Wharton, Major, USAF	
20. DISTRIBUTION/AVAILABILITY OF ABSTRACT UNCLASSIFIED/UNLIMITED <input checked="" type="checkbox"/> SAME AS RPT. <input type="checkbox"/> DTIC USERS <input type="checkbox"/>		21. ABSTRACT SECURITY CLASSIFICATION UNCLASSIFIED	
22a. NAME OF RESPONSIBLE INDIVIDUAL John J. Wharton, Major, USAF		22b. TELEPHONE NUMBER (Include Area Code) 513-255-4498	22c. OFFICE SYMBOL AFIT/ENP

Approved for public release. LAW. APR 1984.
John J. Wharton 13 Feb 86
 JOHN J. WHARTON
 Dean for Research and Professional Development
 Air Force Institute of Technology (AFIT)
 Wright-Patterson AFB OH 45433

UNCLASSIFIED

SECURITY CLASSIFICATION OF THIS PAGE

The purpose of this thesis project was to modify an existing vacuum system into a thin film coating plant which would also employ film thickness monitoring that could be carried out during film deposition for proper control and termination of the process. The thickness monitoring processes employed were the optical method of turning value monitoring, and quartz crystal oscillator frequency monitoring. The results indicated that these two methods responded in the expected manner when a film of TiO_2 was deposited, however, the actual values for the oscillator frequency change and the transmittance at the turning point were not those expected. These errors could be due to a different crystal cut other than AT, or a change in the material index of refraction or chemical composition upon evaporation and subsequent condensation at the substrate. It was recommended, based on the work done during the project, that various equipment upgrades be made and further test deposition runs be accomplished in order to correlate the output of the two monitoring systems.

2
(100)

UNCLASSIFIED

SECURITY CLASSIFICATION OF THIS PAGE

END

DTIC

6-86